

Scalable Quantum Error Mitigation with Neighbor-Informed Learning

Zhenyu Chen^{*1}, Bin Cheng^{*2}, Minbo Gao^{3,4}, Xiaodie Lin^{5,6}, Ruiqi Zhang^{7,8},
Zhaohui Wei^{†7,9}, and Zhengfeng Ji^{‡1,11}

¹Department of Computer Science and Technology, Tsinghua University, Beijing, China.

²Centre for Quantum Technologies, National University of Singapore, Singapore.

³Institute of Software, Chinese Academy of Sciences, Beijing, China

⁴University of Chinese Academy of Sciences, Beijing, China

⁵Department of Mechanical and Automation Engineering, The Chinese University of Hong Kong, Shatin, Hong Kong SAR, China.

⁶College of Computer and Data Science, Fuzhou University, Fuzhou, China.

⁷Yau Mathematical Sciences Center, Tsinghua University, Beijing, China.

⁸Department of Mathematics, Tsinghua University, Beijing, China.

⁹Yanqi Lake Beijing Institute of Mathematical Sciences and Applications, Beijing, China.

¹⁰Zhongguancun Laboratory, Beijing, China.

Abstract

Noise in quantum hardware is the primary obstacle to realizing the transformative potential of quantum computing. Quantum error mitigation (QEM) offers a promising pathway to enhance computational accuracy on near-term devices, yet existing methods face a difficult trade-off between performance, resource overhead, and theoretical guarantees. In this work, we introduce neighbor-informed learning (NIL), a versatile and scalable QEM framework that unifies and strengthens existing methods such as zero-noise extrapolation (ZNE) and probabilistic error cancellation (PEC), while offering improved flexibility, accuracy, efficiency, and robustness.

NIL learns to predict the ideal output of a target quantum circuit from the noisy outputs of its structurally related “neighbor” circuits. A key innovation is our *2-design training* method, which generates training data for our machine learning model. In contrast to conventional learning-based QEM protocols that create training circuits by replacing non-Clifford gates with uniformly random Clifford gates, our approach achieves higher accuracy and efficiency, as demonstrated by both theoretical analysis and numerical simulation. Furthermore, we prove that the required size of the training set scales only *logarithmically* with the total number of neighbor circuits, enabling NIL to be applied to problems involving large-scale quantum circuits. Our work establishes a theoretically grounded and practically efficient framework for QEM, paving a viable path toward achieving quantum advantage on noisy hardware.

1 Introduction

Quantum computing is expected to deliver significant speedups across a variety of computational problems, including quantum simulation [1, 2], integer factorization [3], unstructured search [4], and many other computational problems. However, realizing this promise requires large-scale quantum error correction, which imposes significant resource demands that currently lie far beyond existing technological capabilities. At present, quantum devices operate in the noisy intermediate-scale quantum (NISQ) era, where the qubit count remains insufficient for quantum error correction and the systems are significantly affected by noise [5]. Consequently, it would be desirable to mitigate

^{*}These authors contributed equally to this work.

[†]Corresponding author. Email: weizhaohui@gmail.com

[‡]Corresponding author. Email: jizhengfeng@tsinghua.edu.cn

the impact of noise in quantum information processing tasks with techniques that do not entail substantial quantum overheads. In recent years, a widely applied approach of this kind is the so-called *quantum error mitigation* (QEM) [6, 7, 8].

The two most prominent quantum error mitigation techniques are zero-noise extrapolation (ZNE) [6, 7] and probabilistic error cancellation (PEC) [6]. Several additional quantum error mitigation methods have also been developed, including symmetry verification [9, 10], purification-based approaches [11, 12, 13], and machine learning based techniques [14, 15, 16, 17]. Specifically, ZNE enhances the accuracy of quantum computation by artificially amplifying the noise in a quantum circuit and then extrapolating the noisy outputs back to the zero-noise limit. This approach is appealing due to its low experimental overhead, and has been experimentally demonstrated on superconducting devices [18, 19]. However, its accuracy is ultimately constrained by the quality of extrapolations, and offers little flexibility for further improvement with additional computational resources. The PEC method directly mitigates noise by inverting each noise channel through a quasiprobability decomposition into physically implementable operations [6]. It can, in principle, yield unbiased estimates and has been shown to be theoretically optimal in certain settings [20, 21, 22]. Yet, PEC suffers from a fundamental scalability barrier, i.e., it requires an exponential number of circuit evaluations to suppress noise to high precision. Moreover, it typically depends on accurate noise characterization, which is often difficult to obtain in practice. To address the overhead issue of PEC, heuristic strategies have been proposed, such as truncating the inverse channel expansion and applying learning-based methods to estimate mitigation coefficients [16, 23]. While promising, these approaches generally lack rigorous performance guarantees and are typically benchmarked only on small-scale instances or specific classes of quantum circuits.

In many practical applications of near-term quantum algorithms, achieving higher accuracy is often a priority, and allocating additional computational resources to improve precision can be well justified. This motivates the following fundamental question: *Is it possible to design a quantum error mitigation strategy that is flexible—allowing resource allocation to be dynamically adjusted based on the desired accuracy; efficient—circumventing the computational overhead inherent in methods such as probabilistic error cancellation (PEC); and theoretically sound—with provable performance guarantees under reasonable assumptions?* In this work, we provide an affirmative answer to this question. Specifically, we introduce a general and principled framework for quantum error mitigation, termed neighbor-informed learning (NIL), and demonstrate its strong potential to address these challenges effectively. Much like a detective solving a case by interviewing witnesses rather than confronting the suspect directly, NIL reconstructs the ideal output of a target circuit by aggregating observations from its surrounding neighbor circuits, which offer noisy and partial reflections of the original circuit. Our method is illustrated in Fig. 1 and described in detail in Section 2.

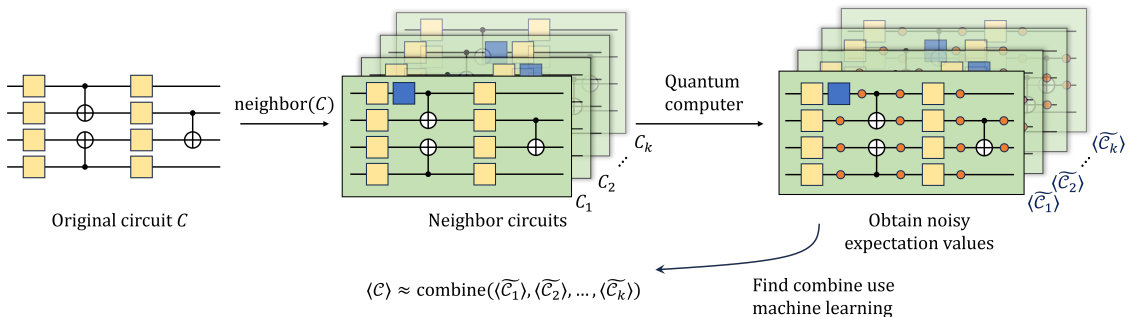


Figure 1: Schematic illustration of NIL. The single-qubit gates in the original circuit are represented by yellow blocks, the inserted gates are represented by blue blocks, and the orange circles represent the noise channels. The noisy expectation values $\langle \tilde{C}_j \rangle$ are obtained on a real quantum device. The function `combine` is learned on a classical computer from a training set of Clifford circuits, for which the ideal expectation values can be efficiently calculated classically.

This strategy provides substantial flexibility in the design of both the neighbor circuits and the learning model, making it broadly compatible with families of parameterized quantum circuits

commonly used in NISQ algorithms such as VQE [24, 25, 26, 27] and QAOA [28, 29, 30]. In particular, we explore a variety of neighbor constructions including gate-insertion schemes that yield Pauli and CPTP-basis neighbor circuits, as well as those inspired by ZNE. We find that combining different types of neighbor circuits can further enhance performance while reducing computational cost. Moreover, we would like to stress that by training our model once on a representative set of training circuits, the learned model can be reused across many circuits of the same configuration.

As a learning-based method, the performance of NIL depends heavily on the quality of training datasets. To this end, we propose a novel *2-design training* strategy tailored for quantum circuit architectures with rotational parameters of quantum gates. The key idea is to replace each non-Clifford gate in the target circuit with a random Clifford gate forming a rotational 2-design, rather than using uniformly random Clifford gates as suggested by the random Clifford method adopted in previous works [16]. We show that the data collected from these training circuits can be used to train an optimal map `combine` selected among the class of linear functions in an average-case sense. In particular, this 2-design training method demonstrates strong generalization ability when linear regression or Lasso regression is used to learn the `combine` map.

Furthermore, we prove that to compute the target expectation value within an error ε , the size of the training set required scales as $\mathcal{O}(\ln N/\varepsilon^2)$, where N is the number of neighboring circuits. This enables the method to leverage a large number of neighbor circuits, which typically enhances the quality of the estimation and improves both efficiency and flexibility. Notably, our bound on the training set size also incorporates the effect of measurement shot noise. We rigorously analyze the error introduced by shot noise and show that the number of measurement shots required is only $\mathcal{O}(1/\varepsilon^2)$. Additionally, we demonstrate that shot noise can have a beneficial regularizing effect on the method.

Through extensive numerical simulations, we demonstrate that, compared to various existing QEM techniques, our method achieves a superior tradeoff between error mitigation performance and computational resource consumption. For example, when applied to the VQE circuits for the LiH molecule, our method achieves a four-order-of-magnitude improvement in MSE at the same training cost, compared to the random Clifford training method [15, 16, 17]. Moreover, we validate the scalability of our method on circuits with over 100 qubits and more than 20 layers, demonstrating that decent QEM performance is still achievable even at scale. Several other technical design choices, such as the construction of neighbor circuits and the selection of learning models and algorithms, are also considered numerically. Additional details can be found in the Appendix.

2 Neighbor-Informed Learning

General framework. Figure 1 illustrates the workflow of NIL. As a general and flexible framework for QEM, NIL reconstructs ideal expectation values by leveraging noisy outcomes from structurally related circuits, referred to as *neighbor circuits*. Instead of relying solely on the noisy outcome of a target circuit \mathcal{C} , NIL collects noisy outcomes from a set of modified circuits $\{\mathcal{C}_1, \dots, \mathcal{C}_N\}$ and uses a learned function `combine` to approximate the ideal result:

$$\langle \mathcal{C} \rangle \approx \text{combine}(\langle \tilde{\mathcal{C}}_1 \rangle, \dots, \langle \tilde{\mathcal{C}}_N \rangle).$$

Here, $\langle \mathcal{C} \rangle$ denotes the ideal, noise-free expectation value of the target circuit \mathcal{C} , while $\langle \tilde{\mathcal{C}}_j \rangle$ represents the noisy expectation value obtained from the j -th neighbor circuit on a quantum device. This formulation generalizes and unifies several existing QEM approaches. For example, in ZNE, neighbor circuits are created by artificially amplifying noise, and `combine` corresponds to an extrapolation function [6, 31]. In PEC, neighbor circuits are generated by inserting physically implementable operations into the original circuit according to quasiprobability distributions that invert the noise channels, and `combine` is the corresponding weighted sum [20].

To implement NIL in practice, we introduce several strategies to construct neighbor circuits: (i) inserting single-qubit gates after noisy operations (referred to as Pauli or CPTP neighbors), and (ii) generating ZNE-style neighbors by scaling the noise rate (see Section 6 for detailed constructions).

For a quantum circuit, the noisy outputs from its neighbor circuits serve as the features of this circuit, which will be utilized in our machine learning models.

2-design training method. The function `combine` is determined using machine learning methods and therefore requires a high-quality training dataset. A central challenge in learning-based QEM is generating training data that statistically mirrors the target circuits, which often feature continuous rotational parameters. To address this, we propose the *2-design training method*, which faithfully respects this rotational parametrization structure. This new method outperforms the conventional *random Clifford* training method widely used in learning-based QEM [15, 16, 17]. While the Clifford training method constructs training circuits by replacing each non-Clifford single-qubit gate with a uniformly random Clifford gate, our method replaces each rotation gate $R_P(\theta)$ with a Clifford gate uniformly drawn from the four-element set $\{R_P(0), R_P(\pi/2), R_P(\pi), R_P(3\pi/2)\}$ where $P \in \{X, Y, Z\}$ is a Pauli operator. The selection of these four Clifford gates is motivated by a key mathematical property that we observe: they constitute a quantum *rotational 2-design* that captures the second-order statistical properties of Pauli rotations $R_P(\theta)$, with θ uniformly distributed over $[0, 2\pi]$. A formal definition and mathematical characterizations of this 2-design construction are provided in Appendix B.

In this work, we assume that target circuits consist of Pauli rotation gates and Clifford gates, which together form a universal set. The training circuits generated by the 2-design method remain Clifford circuits. For each training circuit, we generate its noisy neighbor circuits and collect their outputs as features. The ideal expectation value of the training circuit, which is classically simulable due to its Clifford structure [32, 33], serves as the label.

By repeating this procedure, we construct a sufficiently large training dataset. We then apply linear models to fit the data and obtain a linear estimator of the ideal expectation value for QEM, which will be ultimately applied to the target quantum circuit. Among various types of linear models, we find that *Lasso regression* offers the best trade-off between prediction accuracy and computational efficiency. The 2-design training method is described in detail in Appendix A.

3 Mathematical Characterizations of NIL

Provable optimality. NIL offers several appealing practical advantages for QEM. First, we prove that NIL always achieves the optimal performance across all linear models, regardless of the presence of shot noise. The proof relies on the observation that, when reformulating the linear regression problem as a quadratic optimization problem, each entry of the resulting coefficient matrix can be expressed as the trace of a second-moment expression involving the rotation gates $R_P(\theta)$ and $R_P(-\theta)$. Notably, the statistical properties of these coefficients can be mimicked by their behavior at the specific rotation angles $\{R_P(0), R_P(\pi/2), R_P(\pi), R_P(3\pi/2)\}$. This implies that in the large size limit, the training set matches the test set on average, and the solution to the linear (or Lasso) regression exhibits excellent generalization capabilities.

Theorem 1 (informal). *As the size of the training set approaches infinity, the linear model trained with the 2-design training method converges to the optimal linear estimator for the target circuits.*

The detailed proof of Theorem 1 is provided in Appendix B. We establish this result under both noiseless and shot-noise-affected expectation value settings.

Limitation of the Clifford training method. Since single-qubit rotational gates with parameters are prevalent in many near-term quantum algorithms, the 2-design training method offers broad applicability and practical relevance. Importantly, we prove that the 2-design training method is provably superior to the Clifford training method. The former is not only more efficient and accurate, but also resolves a key limitation of the latter: In the Clifford training method, the mean squared error (MSE) obtained on the training dataset fails to converge to the corresponding value on the target circuit in the average sense, and as a result, the generalization error of the model is non-negligible, seriously limiting its performance.

On the other hand, if we generate the training dataset with the 2-design training method, the MSE of any linear model evaluated on the training dataset exactly matches the MSE on the target

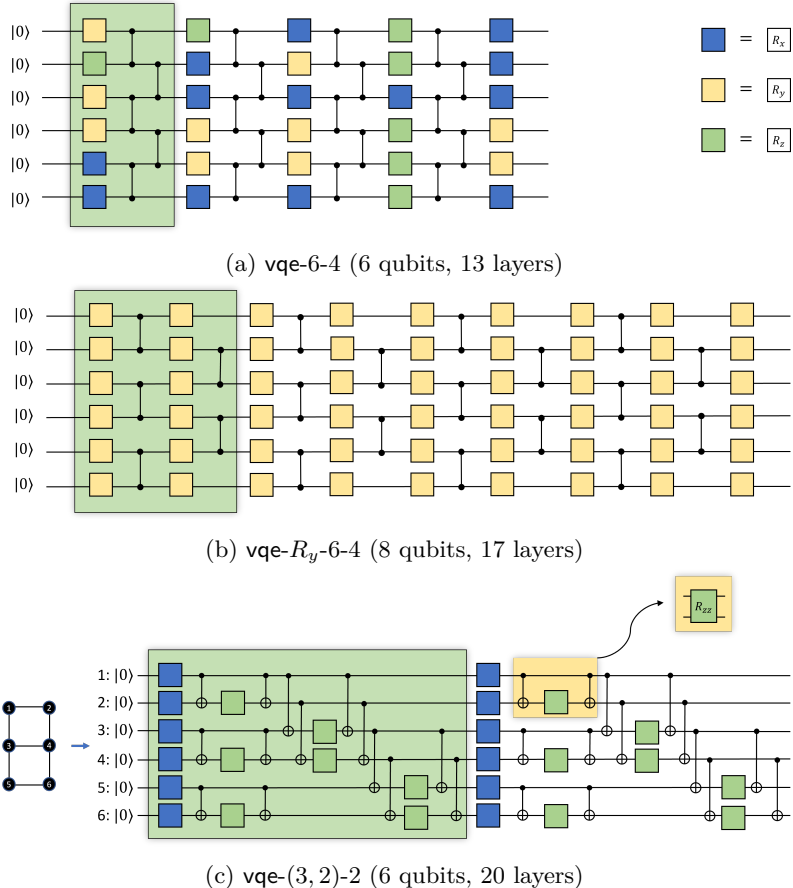


Figure 2: Three types of ansatz circuits we employ to test NIL. In these diagrams, colored boxes represent single-parameter rotation gates, vertical black lines are two-qubit Clifford gates, and the areas enclosed by dashed lines denote a complete block. All three circuits contain six qubits and can be extended to an arbitrary number of qubits.

parameterized quantum circuit. This crucial equivalence ensures the advantage of our approach over the Clifford training method that is widely applied in the literature. Furthermore, we would like to remark that this property also allows us to benchmark the performance of our approach on large-scale target quantum circuits that are hard to simulate classically, as it only requires us to compute the ideal expectation values for Clifford training circuits. The proof of this property can be found in Appendix D.

Scalability and efficiency of NIL. We now analyze the size of the training dataset required to obtain a reliable linear estimator for practical deployment. We prove that using Lasso regression with a constraint on the ℓ_1 -norm of the linear estimator, our model requires only a *logarithmic* number of training circuits in N , the number of neighbor circuits. This ensures that a good estimator can be learned efficiently for mitigating noise in the target circuit, supporting scalability to large-scale quantum circuits. Additionally, we derive the classical runtime of NIL, showing its time complexity remains polynomial in N . The detailed derivations are provided in Appendix C. These properties collectively establish NIL as a scalable and practical approach for QEM.

NIL possesses several additional noteworthy properties. First, when examining the effect of shot noise caused by quantum measurements, we find that its presence introduces an additional helpful regularization term into the original linear regression problem from a statistical perspective. This implies that a small amount of shot noise, which is common in practical scenarios, can actually enhance the numerical stability of the linear regression. Moreover, we rigorously prove that to obtain a linear estimator with an additive error ε with NIL, the number of measurement shots

required for estimating each noisy neighbor circuit's expectation value is $\mathcal{O}(1/\varepsilon^2)$. Combining these facts, we have the following theorem.

Theorem 2 (informal). *When using the 2-design method to generate the training set in NIL, it suffices to choose the size of the training set T to be $\mathcal{O}(\ln N/\varepsilon^2)$ to achieve an error of ε in MSE.*

The detailed proofs are provided in Appendix B and Supplementary Appendix C.

4 Numerical Simulations and Comparison

We now illustrate the effectiveness of NIL in QEM by benchmarking it against existing QEM methods. First, we provide numerical evidence supporting our theoretical result that unlike the Clifford training method, NIL consistently converges to the optimal linear estimator. Second, motivated by the recent seminal experimental work [34] demonstrating the power of the ZNE protocol in QEM, we show that its performance can be further enhanced by integrating our approach.

We first conduct numerical experiments on several small-scale variational quantum algorithms, for which the ideal expectation values of the circuits can be classically simulated. With access to the exact outputs of these non-Clifford circuits, we are able to compare the performance of NIL with that of conventional QEM methods such as ZNE. We examine three representative circuit types: variational ansatz circuits for 1D and 2D transverse-field Ising (TFI) models, and unitary coupled-cluster (UCC) circuits for simulating the LiH molecule. Unless stated otherwise, the noise model applied is local depolarizing noise with a strength of 0.001 for single-qubit gates and 0.01 for two-qubit gates. Importantly, our method does not require prior knowledge of the noise model and thus remains applicable to arbitrary noise models in practical settings.

1D and 2D transverse-field Ising model. Variational Quantum Eigensolver (VQE) is a class of hybrid quantum-classical algorithms designed to find the minimum eigenvalues of Hamiltonians, which has been widely applied in quantum chemistry and physics [24, 25, 26, 27]. The basic workflow of VQE involves preparing a quantum state using a quantum circuit with tunable parameters (called the ansatz circuit), measuring the energy of the system, and then using a classical optimizer to iteratively adjust the circuit parameters to minimize the energy. Here, we use VQE as a testbed for our NIL technique.

Specifically, we consider two classes of target problems: the transverse-field Ising (TFI) model and a quantum chemistry problem. Given a graph $G = (V, E)$, the TFI Hamiltonian is defined as

$$H_{\text{TFI}} = -J \sum_{(i,j) \in E} Z_i Z_j - h \sum_{j \in V} X_j,$$

where we set $J = 1$ and $h = 2$. We consider two different graphs: a 1D line and a 2D grid.

For the 1D case, we choose two kinds of hardware-efficient ansatz [27, 16]. The first one, labeled as `vqe-n-m` and depicted in Fig. 2 (a), involves applying the block enclosed by the red dotted line m times, where n is the number of qubits. Inside a block, there is a layer of random Pauli rotations in the X , Y , or Z direction and a layer of CZ gates. The second one, labeled as `vqe-Ry-n-m` and depicted in Fig. 2 (b), has a similar structure, but in this case there are two layers of Pauli-Y rotations and two layers of CZ gates inside a block.

For the 2D case, we choose the so-called Hamiltonian variational ansatz (HVA) [35]. For an $n_1 \times n_2$ grid, the ansatz circuit is labeled as `vqe-(n1, n2)-m` and defined by

$$\prod_{t=1}^m \exp \left(i \sum_{j \in V} \alpha_j^{(t)} X_j \right) \exp \left(i \sum_{(j,k) \in E} \beta_{jk}^{(t)} Z_j Z_k \right);$$

see Fig. 2 (c) for an example. Note that unlike the original HVA, here we let all the angles in the rotation gates be tunable.

On these problems we first compare the performance of NIL with that of the learning-based QEM protocol introduced in Ref. [16]. For this, we adopt the neighbor generation strategy proposed

therein: inserting random Pauli operators at up to three randomly selected positions in both the training and the target circuits. We refer to the resulting circuits as *weight-3 neighbors*, detailed construction and discussion are provided in Section 6. Based on this set of neighbor circuits, we prepare two training datasets of size 5,000 each: one generated via the 2-design training method, and the other via the Clifford training method that replaces each non-Clifford single-qubit gate by uniformly random Clifford gates. Lasso regression is used to produce a linear estimator for QEM separately on each dataset.

To evaluate and compare the performance of the obtained linear estimators for QEM, we construct a test set of 1,000 non-Clifford circuits with rotation angles uniformly sampled from $[0, 2\pi]$. We generate corresponding neighbor circuits for these test circuits with the same strategy as for the training circuits, then collect the noisy expectation values for them as features and obtain the ideal expectation values as labels via classical simulations. Then we apply the two linear estimators obtained by 2-design training method and the Clifford training method on the test dataset, and the corresponding MSEs can be seen in Fig. 3. Note that to benchmark the performance of the two linear estimators, we also apply Lasso regression directly to fit the test dataset, and obtain a third linear estimator.

In Fig. 3 it can be seen that the MSE of the estimator learned from NIL (blue curve) consistently decreases as the number of neighbor circuits increases. Moreover, the blue curves closely follow the linear estimator learned directly from the test dataset (green curve), providing strong empirical support for our theoretical claim that NIL can accurately approximate the optimal linear model. In contrast, the Clifford training method (orange curve) consistently yields higher test error.

Meanwhile, it can be observed that using only weight-1 neighbors—whose number equals the number of gates in the target circuit—already yields sufficiently low MSE, making it practical for QEM. When restricting to weight-1 neighbors, NIL achieves approximately half the MSE of the Clifford training method for VQE circuits for the 1D TFI Hamiltonian, and an advantage of one order of magnitude for the 2D TFI Hamiltonian. These results confirm once again that, for the target circuits considered, NIL outperforms the Clifford training method in QEM performance.

We further evaluate the performance of NIL in combination with the ZNE protocol [34]. For a fair comparison, NIL chooses all the neighbor circuits as ZNE neighbors (see Section 6 for details), using the same 5,000 training circuits generated previously. The resulting linear model is then applied to the 1,000 non-Clifford test circuits generated previously. For the ZNE approach, we apply the same protocol as in Ref. [34] (see Section 6 for details) to the same set of test circuits and compute the MSE between the mitigated and the ideal expectation values.

The comparison results are summarized in Table 1. It can be seen that NIL with ZNE neighbors consistently outperforms the original ZNE protocol across all the test circuits, further demonstrating the power of our approach. It is worth noting that, as a flexible machine-learning-based approach, NIL enables further improvement of the ZNE protocol by incorporating different types of neighbor circuits. A detailed comparison and application of this approach are provided in the Appendix H.

Circuit	NIL	ZNE
vqe-6-4	1.82×10^{-6}	1.09×10^{-4}
vqeRy-6-4	3.80×10^{-6}	1.56×10^{-4}
vqe-3-2-2	1.31×10^{-6}	1.92×10^{-4}
vqe-8-4	2.63×10^{-6}	1.58×10^{-3}
vqeRy-8-4	5.78×10^{-6}	3.52×10^{-3}
vqe-4-2-2	4.11×10^{-6}	3.63×10^{-3}

Table 1: Comparison of NIL and ZNE performance. Test MSE for NIL using ZNE neighbors versus the standard ZNE protocol on various VQE circuits. NIL consistently achieves an error reduction of two orders of magnitude.

UCC ansatz circuits for LiH. We also consider a quantum chemistry problem, i.e., we choose the UCC ansatz to study the LiH and F₂ molecules [24] (see Appendix I for the circuit diagram). As in [36], we adopt a series of simplification strategies for this problem, such as imposing the point group symmetry constraint. The description of the Hamiltonian and the ansatz circuit

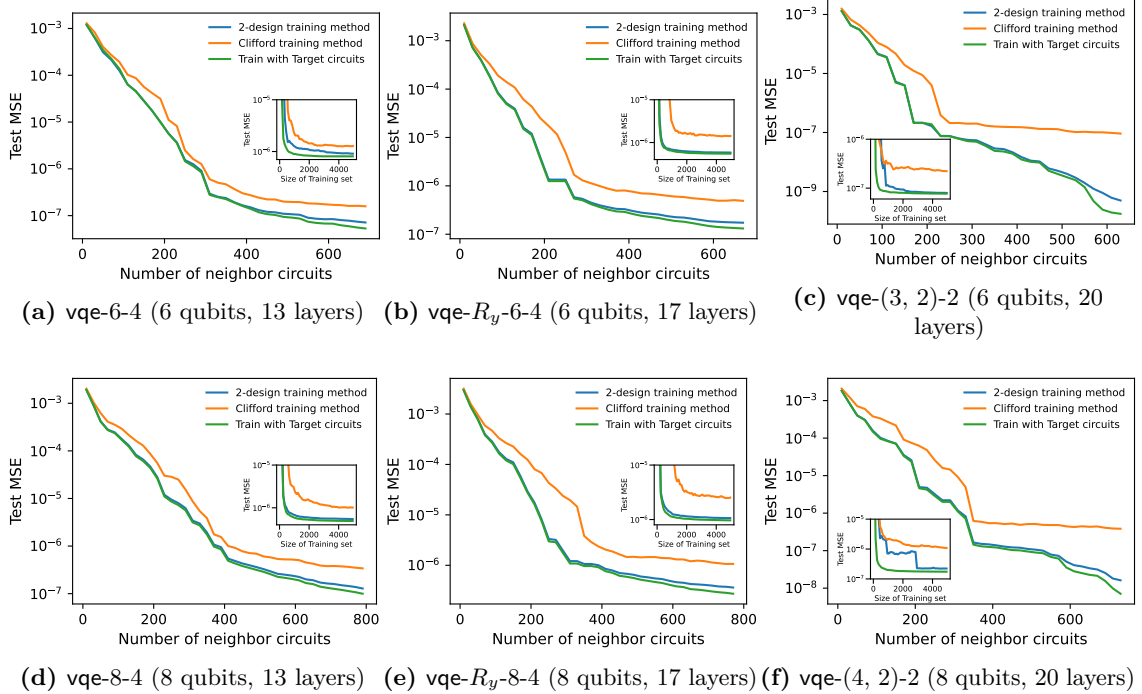


Figure 3: Performance of learning-based QEM protocols using different sets of training circuits. The blue curve shows the MSE of the solution obtained via NIL, the green curve corresponds to the solution from direct fitting on the test dataset, and the orange curve represents the solution using the Clifford training method. The inset illustrates the decrease in MSE as the size of the training set increases, with neighbor circuits selected as all weight-1 neighbors.

after simplification can be found in Appendix I. Compared to the TFI Hamiltonian, molecular Hamiltonians from quantum chemistry are generally more complex, where the number of terms scales as $O(n^4)$ [37].

For this case, we first employ Pauli-insertion neighbors to compare the performance of NIL with that of the Clifford training method [16], following the same procedure as before. Since this circuit has only four parameterized rotation gates, NIL requires a training dataset of size $4^4 = 256$. In sharp contrast, a complete training dataset of size 24^4 is required for the Clifford training method. Similarly, we generate 1,000 non-Clifford circuits to construct a test set for evaluating the learned linear estimators. In addition, we apply Lasso regression directly to these 1,000 test circuits to obtain a reference linear estimator, aiming to verify whether our method can learn a model that converges to the actual optimal one.

As shown in Fig. 4, the MSE of the linear model obtained by our method (blue curve) on the test dataset decreases continuously to a value close to zero as the number of neighbor circuits increases. Furthermore, its MSE curve almost overlaps with that of the linear estimator directly fitting the test dataset (green curve), clearly demonstrating the strong generalization capability and the excellent QEM performance of our approach. Remarkably, as we can see in the inset of Fig. 4, NIL achieves a 4 order magnitude improvement over the Clifford training method when the models employ all the weight-1 neighbor circuits.

Another crucial observation here is that as the number of neighboring circuits increases, our approach consistently leads to better QEM performance. This occurs because our solution converges to the optimal linear estimators, and thus more neighbor circuits naturally reduce the obtained MSE on the target circuit. However, this is not necessarily true for the Clifford training method. As shown by the orange curve in Fig. 4, the performance of the Clifford training method is not even stable. This confirms that the results given by the Clifford training method contain systematic errors. In fact, we find that the linear estimator trained using the Clifford training method actually converges to the optimal linear QEM strategy for a different class of target circuits (see Appendix G

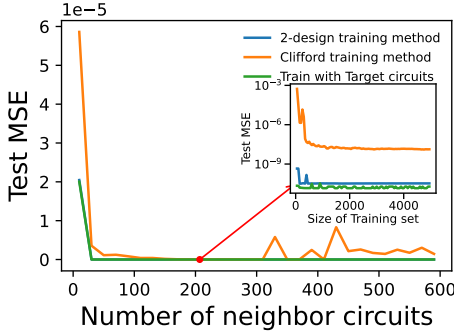


Figure 4: Performance of learning-based QEM protocols using different methods for generating training sets. The underlying circuit is the 6-qubit UCC ansatz circuit for LiH.

for details), which explains the observed bias.

Finally, we compare the performance of the ZNE protocol and that of NIL on this problem. The ZNE implementation again follows Ref. [34], while NIL is trained using the 2-design method with ZNE neighbors, followed by Lasso regression to obtain a linear estimator. For the 1,000 test circuits generated previously, the ZNE method yields an MSE of 1.23×10^{-4} , whereas NIL with ZNE neighbors achieves an MSE of 2.22×10^{-8} —a four-order-of-magnitude improvement.

Based on our data in this case, achieving chemical accuracy (approximately 6.6×10^{-4} [38, 39], corresponding to a squared error below 4.3×10^{-7}) requires only four ZNE neighbor circuits to construct the neighbor map. This example illustrates that for quantum circuits with relatively few parameters, our method delivers excellent QEM performance with a small training cost. Furthermore, for the 12-qubit UCC ansatz of the F_2 molecule, we apply our NIL method and find that using only half of the weight-1 Pauli neighbors suppresses about 99% of the errors. Further details are provided in Appendix I.

5 Scalability to Large Quantum Circuits

A major challenge for learning-based QEM is benchmarking its performance on circuits that are too large to simulate classically. Our framework addresses this through a crucial theoretical result (Supplementary Appendix D), which guarantees that the average MSE on the training set is identical to that on the test set. This equality allows us to reliably benchmark NIL’s performance on classically intractable systems by evaluating it on the efficiently simulable Clifford training circuits.

We first test our approach on the `vqe-(5,4)-2` circuit, which is for the 2D transverse-field Ising model and consists of 20 qubits and 26 layers. We employ all weight-1 Pauli neighbors as the set of neighbor circuits and generate 1,000 training circuits using the 2-design training method. Then we calculate the noisy expectation value for each neighbor circuit with 10,000 shots (see Section 6 for details) and apply Lasso regression to fit the training dataset. The results are shown in Fig. 5a. It can be seen that the training MSE (\approx test MSE) for this 20-qubit circuit is very small, demonstrating that our method works well in this case.

Lastly, we evaluate the performance of our approach on a 100-qubit circuit `vqe-Ry-100-5`, which consists of 21 layers. Here we use at most 200 random weight-1 Pauli neighbors and generate 1,000 training circuits via the 2-design training method. The training procedure remains the same as in previous experiments. As shown in Fig. 5b, our method achieves an excellent performance, further validating the effectiveness of our approach on large-scale quantum circuits.

Notably, the overall sampling overhead for these three cases amounts to at most 6×10^9 shots, which represents a reasonable cost for state-of-the-art superconducting quantum platforms, as estimated in [8]. With this overhead, we achieve at least one order of magnitude of error mitigation improvement. In particular, for the 12-qubit UCC ansatz circuit of F_2 , the mitigation gain approaches nearly two orders of magnitude. These results demonstrate that NIL can deliver excellent error mitigation performance on large-scale circuits at experimentally feasible costs.

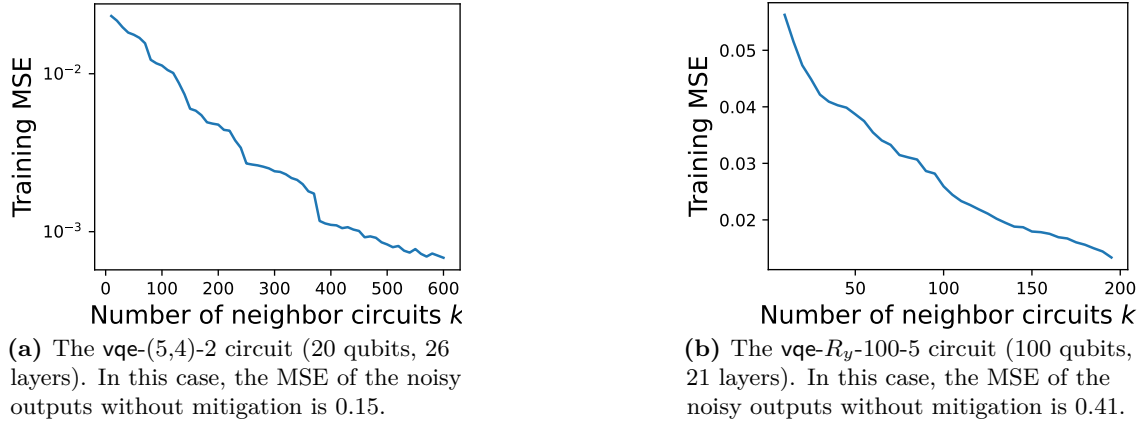


Figure 5: Performance of NIL on large-scale quantum circuits.

6 Implementation Details

Pauli insertion neighbor circuits. For a given target quantum circuit, inspired by PEC, a natural strategy to construct neighbor circuits is to perturb the original circuit by inserting a set of gates from a certain set \mathbb{G} into C . For example, when inserting a gate $P \in \mathbb{G}$ after the single gate U_j , it will be replaced by PU_j , while the rest of the circuit remains unchanged. To recover the ideal expectation value, a learning-based QEM protocol needs to collect the noisy expectation values from all circuits $\{\tilde{C}_j\}_j$, which are obtained by inserting gates from \mathbb{G} after specific gates in the original circuit C .

For Pauli insertion neighbor circuits, $\mathbb{G} := \{\mathcal{X}, \mathcal{Y}, \mathcal{Z}\}$, the same as the learning-based PEC approach [16]. In the language of NIL, the original PEC approach uses a number of neighbor circuits that is exponential in the number of noise positions. To make the error mitigation scheme resource-efficient, Ref. [16] proposed a truncation strategy that only keeps the low-weight neighbor circuits, where a weight- ℓ neighbor circuit is constructed by inserting quantum gates after at most ℓ positions of the original circuit. In what follows, we also generate neighbor circuits by inserting gates after noisy operations, and we similarly restrict our attention to the low-weight case. Specifically, weight- m Pauli neighbors refer to circuits where a Pauli gate is inserted after at most m noisy gates. For a quantum circuit C with m possible noise positions, the set of weight-1 neighbor circuits is of size $O(m)$, and the set of weight-2 neighbor circuits is of size $O(m^2)$. In practice, the number of weight-2 neighbor circuits can already be prohibitive, even for modest-sized quantum circuits with $m \sim 10^3$ gates. Therefore, we need a more flexible strategy to choose neighbor circuits than the simple truncation strategy.

For this purpose, we introduce a randomized approach for selecting neighbor circuits. For instance, to construct a scheme with s neighbor circuits, where s is smaller than the total number of all weight-1 neighbor circuits, we randomly select s circuits from the weight-1 neighbor circuits as the chosen set. This approach enables the error mitigation scheme to adapt to the tolerable experimental cost.

Lasso regression. Lasso regression [40] is a special form of linear regression that adds an ℓ_1 -norm constraint on the coefficients that need to be optimized. Suppose the training set is

$$\mathbb{S} = \left\{ \left(\left(x_1^{(i)}, \dots, x_N^{(i)} \right), y^{(i)} \right) \right\}_{i=1}^T,$$

then Lasso regression solves the following optimization problem:

$$\begin{aligned} \min_{c_1, \dots, c_N} \quad & \frac{1}{T} \sum_{i=1}^T \left(\sum_{j=1}^N c_j x_j^{(i)} - y^{(i)} \right)^2 \\ \text{subject to} \quad & \sum_{j=1}^N |c_j| \leq \gamma. \end{aligned} \tag{1}$$

where $\gamma > 0$ is the regularization. In our numerical calculations, we solve the above convex optimization problem using `CVXPY` [40], with `MOSEK` [41] as the backend solver due to its high precision and robustness for large-scale convex programs.

To control the sparsity of the learned coefficients, we use Lasso regression with different regularization strengths depending on the type of neighbor circuits. Specifically, we set $\gamma = 5$ when using ZNE-based neighbor circuits, and $\gamma = 2$ for all other neighbor circuit constructions. This choice helps to reduce the ℓ_1 norm of the solution while maintaining strong QEM performance.

ZNE implementation. The ZNE protocols considered include exponential extrapolation and linear extrapolation, both implemented via `mitiq` [42]. As noted in [34], exponential extrapolation suffers from numerical instability in some cases. When this is the case, we fall back to using linear extrapolation.

ZNE neighbor circuits. We also propose a neighbor map construction method inspired by ZNE. Recall that in ZNE protocols, neighbor circuits are obtained by amplifying all noise channels, i.e., effectively replacing each noise channel Λ with Λ^α . In this work, following the noise extrapolation approach of [34], we choose $\alpha \in \{1, 1.1, 1.34, 1.58\}$. We refer to the neighbor circuits constructed using this method as *ZNE neighbor circuits*. In subsequent work [43], we systematically compare the performance under different noise amplification rates and demonstrate that our approach substantially improves the accuracy of variational quantum algorithms.

Expectation value estimation. For large-scale quantum circuits, we estimate the expectation values of observables by executing the circuit multiple times and averaging the measurement outcomes. To reduce experimental overhead and facilitate implementation, we employ Pauli basis measurements. Specifically, the target observable is first decomposed into a linear combination of Pauli operators. For example, the TFI Hamiltonian can be written as

$$H_{\text{TFI}} = -J \sum_{(i,j) \in E} Z_i Z_j - h \sum_{j \in V} X_j. \tag{2}$$

We then group mutually commuting Pauli terms so that each group can be measured simultaneously using a single measurement basis. In the case of the TFI Hamiltonian, the decomposition yields two commuting groups: $\{Z_i Z_j\}_{(i,j) \in E}$ and $\{X_j\}_{j \in V}$. To estimate the overall expectation value, we allocate an equal number of measurement shots to each group. For instance, using 10,000 total shots, we assign 5,000 shots to each group. Since the training circuits considered in our study are Clifford circuits subject to Pauli noise, all measurement data can be efficiently generated using Clifford simulators `stim` [44].

7 Discussions

We have introduced NIL, a general and scalable framework for learning-based QEM. At its core is a principled strategy for constructing sets of training circuits based on quantum 2-designs. We have also proven that this strategy yields the optimal linear estimator in an average sense. By employing Lasso regression, we are able to reduce the quantum sampling cost and show a theoretical understanding for scalability of NIL: to achieve an estimator with MSE within ε of the optimum with confidence $1 - \delta$, it suffices to use $\mathcal{O}(\ln(N/\delta)/\varepsilon^2)$ training circuits, where N is the number of features (neighbor circuits). This scaling makes the method efficient and

realistic even for large-scale quantum circuits. Numerical simulations on variational quantum circuits—including 1D and 2D transverse-field Ising models and molecular Hamiltonians like LiH—demonstrate the strong empirical performance of NIL. We have also compared different neighbor circuit generation strategies, and find that Pauli insertion neighbors consistently outperform CPTP-basis constructions.

Interestingly, an important and valuable feature of our framework lies in its applicability to circuits that are beyond classical simulations. We have shown that NIL can be reliably evaluated even on quantum circuits with 20 to 100 qubits or more, thanks to a theoretical guarantee equating the average MSE on the set of Clifford training circuits to the MSE on target circuits, under mild assumptions. This enables benchmarking of learning-based QEM schemes on classically intractable systems—an important step toward practical deployment.

While our analysis has focused on linear models and the MSE loss function, several questions remain open. Although we provide theoretical and numerical evidence that a low MSE implies reliable mitigation with high probability for any specific circuit instance (Appendix E), the relationship between average-case and worst-case performance warrants further investigation. Additionally, while our tests with neural networks did not show an advantage over linear models (Appendix H), the potential benefits of more sophisticated non-linear models in different noise regimes or for different tasks remain an interesting direction for future research.

In conclusion, NIL provides a theoretically grounded, practically efficient, and scalable framework for quantum error mitigation. By unifying concepts from existing methods and leveraging a provably optimal learning strategy, it offers a viable path toward extracting reliable results from today’s noisy quantum hardware and advancing the pursuit of quantum advantage.

Supplemental Material

Contents

1	Introduction	1
2	Neighbor-Informed Learning	3
3	Mathematical Characterizations of NIL	4
4	Numerical Simulations and Comparison	6
5	Scalability to Large Quantum Circuits	9
6	Implementation Details	10
7	Discussions	11
A	Implementation Details of the 2-Design Training Method	14
A.1	Target Quantum Circuits	14
A.2	Data Generation Method	15
A.3	Loss Function and Learning Models	15
B	Optimality of the 2-Design Training Method	16
B.1	Quantum Rotation t -design	17
B.2	Asymptotic Optimality	18
B.2.1	Optimality without Shot Noise	18
B.2.2	Optimality with Shot Noise	21
C	Estimation of the Computational Cost	26
C.1	Estimation of the Size of Training Set	26
C.2	Time Complexity of NIL	29
D	Benchmarking Performance on Large-scale Non-Clifford Circuits	30
E	Mean Squared Error and Worst Case Error	31
E.1	Low Mean Squared Error May Indicate Low Worst-Case Error	32
F	Using Non-Clifford Quantum Circuits for Training	33
F.1	Comparison Between Mixed and Purely Clifford Training Circuits	34
G	Producing Training Circuits with All the Single-Qubit Clifford Gates	34
H	Comparisons Between Different Design Choices of NIL-based QEM	36
H.1	Comparison Between Choices of Neighbor Maps	36
H.2	Comparison Between Linear Models and Neural Networks	37
I	Quantum Chemistry Problems	38
I.1	Performance of NIL on UCC Ansatz Circuits for F_2	39

A Implementation Details of the 2-Design Training Method

In this section, we present the detailed procedure of the 2-design training method. Suppose that the target quantum circuit is C , and a set of training quantum circuits $S = \{C^{(1)}, C^{(2)}, \dots, C^{(T)}\}$ is constructed, referred to as “training circuits”. For each training circuit $C^{(i)}$, the chosen neighbor circuits is

$$\text{neighbor}(C^{(i)}) = (C_1^{(i)}, \dots, C_N^{(i)}).$$

For each $i = 1, 2, \dots, T$ and $j = 1, 2, \dots, N$, we run the circuit $C_j^{(i)}$ and obtain the noisy target expectation value $\langle \widetilde{C}_j^{(i)} \rangle$. Then, the whole training data for \mathbb{S} can be written as

$$\mathbb{S} := \left\{ \left(\left(x_1^{(i)}, \dots, x_N^{(i)} \right)^\top, y^{(i)} \right) \right\}_{i=1, \dots, T},$$

where

$$x_j^{(i)} = \langle \widetilde{C}_j^{(i)} \rangle, \quad (3)$$

and

$$y^{(i)} = \langle C^{(i)} \rangle. \quad (4)$$

That is, for each training quantum circuit $C^{(i)}$ in S , the final training data includes the noisy expectation values of all its neighbors, and the noiseless expectation value $\langle C^{(i)} \rangle$ itself. Then, one needs to find a proper function by which the value of $\langle C^{(i)} \rangle$ can be predicted well based on those of $\langle \widetilde{C}_j^{(i)} \rangle$ for all the training data. The hope is that machine learning can capture the pattern of quantum noise, enabling the learned function to predict the ideal expectation value as well on the target quantum circuit C by analyzing the noisy expectation values of all its neighboring circuits.

A key requirement in selecting the training circuits $C^{(i)}$ is ensuring that the noiseless expectation value $\langle C^{(i)} \rangle$ can be computed both precisely and efficiently. A common strategy for this purpose is to choose Clifford training circuits, as they have the desirable property that the exact expectation values $\langle C^{(i)} \rangle$ can be computed efficiently [32, 33].

In learning-based QEM, proper construction of training data is crucial for the success of machine learning models. One of our main contributions in this work is the discovery of an effective strategy, called *2-design training*, that generates training quantum circuits based on the mathematical tool of *t*-design [45]. In particular, we demonstrate that this strategy enables us to efficiently identify the optimal *combine* function among all linear options, outperforming even neural networks in terms of performance.

A.1 Target Quantum Circuits

Before introducing our new approach, we would like to clarify the target quantum circuits (sometimes referred to as “test circuits”) for our QEM task, which are a family of quantum circuits sharing the same structure. These circuits can be written as $C(\boldsymbol{\theta}) = U_m(\theta_m) \cdots U_1(\theta_1)$, where $\boldsymbol{\theta} = (\theta_1, \dots, \theta_m)$, and each θ_i lies in the interval $[0, 2\pi]$. Here, we assume that each unitary operation $U_i(\theta_i)$ is either a single-qubit parameterized rotation gate $R_\sigma(\theta_i)$ with the rotation angle θ_i or a fixed one- or two-qubit Clifford gate F_i without parameters, where $\sigma = x, y, z$ corresponds to the rotation axis. See Fig. 6 for an example. Additionally, after fixing the circuit structure, we assume that the noise models of all quantum gates remain unchanged when θ_i ’s are varied.

This type of quantum circuit is very common for near-term quantum algorithms such as variational quantum algorithms [24, 28], and covers nearly all hardware-efficient variational quantum circuits. In a typical variational quantum algorithm, one often constructs an ansatz circuit $C(\boldsymbol{\theta})$ and adjusts the parameters $\boldsymbol{\theta}$ such that the output of the circuit can approximate the ground state of a Hamiltonian H . Since optimal solutions may appear at any value of $\boldsymbol{\theta}$, our objective is to achieve effective error mitigation for all potential values of $\boldsymbol{\theta}$ at a tolerable cost, rather than to focus on a specific individual circuit or a specific value of $\boldsymbol{\theta}$.

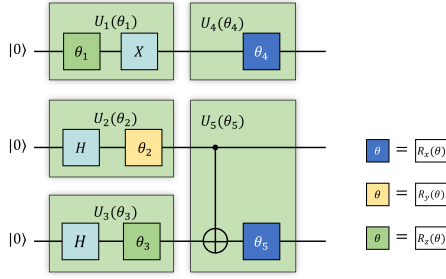


Figure 6: A typical parameterized quantum circuit $C(\theta)$. This circuit contains six parameters and can be represented in the form of $C(\theta) = U_5(\theta_5) \cdots U_1(\theta_1)$, where each $U_i(\theta_i)$ is composed of several gates enclosed within a light green frame. For instance, $U_1(\theta_1) = X R_z(\theta_1)$.

A.2 Data Generation Method

Previous works typically construct the set of training quantum circuits by maintaining the structure of the target quantum circuit while replacing each (single-qubit) non-Clifford gate with a Clifford gate uniformly sampled from all 24 single-qubit Clifford gates [16] (Clifford training method), or from a subset of these Clifford gates [46]. We refer to this strategy for constructing training quantum circuits as the *Clifford training method*, which is a heuristic approach without rigorous performance analysis.

In contrast, the *2-design training* method (2-training method) we propose replaces each non-Clifford gate with one of the *four* gates forming a rotational 2-design, as will be elaborated shortly. Recall that the single-qubit parameterized gates in the target circuits are Pauli rotation gates $R_\sigma(\theta)$ with $\sigma = x, y, z$. The four Clifford gates for each gate $R_\sigma(\theta)$ are $R_\sigma(\theta_0)$, where θ_0 is chosen from $\{0, \pi/2, \pi, 3\pi/2\}$. Besides significantly reducing the computational cost of the training stage, we will demonstrate that the effectiveness of the 2-design training method has a solid theoretical foundation in Section B, and its performance is numerically verified to significantly surpass that of the Clifford training method.

Algorithm 1 Strategy for constructing training circuits with all single-qubit Clifford gates

Input: Target parameterized circuit $C(\theta)$

Output: A set S of training circuits

```

1: repeat
2:   for each gate in the circuit  $C(\theta)$  do
3:     if the gate is of the form  $R_\sigma(\theta)$  ( $\sigma = x, y, z$ ) then
4:       Replace  $R_\sigma(\theta)$  with  $g \in \mathbb{C}_1$  randomly, where  $\mathbb{C}_1$  is the single-qubit Clifford group.
5:     end if
6:   end for
7:   Add the new circuit to  $S$ 
8: until Collect sufficient circuits for training

```

In 2-training method, “ $\leftarrow_{\$}$ ” means “sampled uniformly at random from”. We set the size of the training set T to be sufficiently large so that the loss function (defined later) remains relatively stable during training and converges eventually. In practice, we can gradually increase the size of T , monitor the loss function fluctuations, and add more training circuits if needed.

Additionally, we consider a training set generation method that produces training circuits with a shallow non-Clifford layer, bringing the training circuits closer to the test circuit. See Section F for more details.

A.3 Loss Function and Learning Models

After preparing the training set, we need to train an appropriate function `combine` that fits the training set. The loss function is chosen to be the mean squared error (MSE), which is a widely

Algorithm 2 Strategy for constructing training circuits with quantum rotation 2-design

Input: Target parameterized circuit $C(\theta)$

Output: A set S of training circuits

```
1: repeat
2:   for each gate in the circuit  $C(\theta)$  do
3:     if the gate is of the form  $R_\sigma(\theta)$  ( $\sigma = x, y, z$ ) then
4:        $\theta \leftarrow \{0, \pi/2, \pi, 3\pi/2\}$ 
5:     end if
6:   end for
7:   Add the new circuit to  $S$ 
8: until Collect sufficient circuits for training
```

used metric to quantify the performance of machine learning models and is defined as

$$\text{MSE} := \frac{1}{T} \sum_{i=1}^T \left(y^{(i)} - \hat{y}^{(i)} \right)^2. \quad (5)$$

Here, $y^{(i)}$ is the noiseless expectation value of the i -th training circuit, $\hat{y}^{(i)}$ is the corresponding value predicted by the model, and T is the size of the training set.

In this work, we analyze and compare three learning models designed to minimize the MSE on the training set. We first consider two linear models for `combine`: linear regression and Lasso regression. Specifically, given the training dataset \mathbb{S} , a linear regression solves the following optimization problem:

$$\min_{c_1, \dots, c_N} \frac{1}{T} \sum_{i=1}^T \left(\sum_{j=1}^N c_j x_j^{(i)} - y^{(i)} \right)^2, \quad (6)$$

where c_j 's are the parameters to learn. We solve this problem using the `LinearRegression` function from `sklearn` [47].

It is straightforward to see that Eq. (6) is a Least Squares (LS) problem [48]. However, the ℓ_1 norm of the solution obtained from Eq. (6) can be too large, making the obtained `combine` impractical. To overcome this problem, we use Lasso regression [40], which imposes an ℓ_1 norm constraint on the parameters:

$$\begin{aligned} \min_{c_1, \dots, c_N} \quad & \frac{1}{T} \sum_{i=1}^T \left(\sum_{j=1}^N c_j x_j^{(i)} - y^{(i)} \right)^2 \\ \text{subject to} \quad & \sum_i |c_i| \leq \gamma, \end{aligned} \quad (7)$$

where $\gamma > 0$. In our numerical calculations, we solve the convex optimization problem in Eq. (7) using `CVXPY` [40], with `MOSEK` [41] as the backend solver due to its high precision and robustness for large-scale convex programs.

Using Lasso regression, we can reduce the ℓ_1 norm of the solution by appropriately choosing γ . For instance, in linear regression, the value of $\sum_i |c_i|$ can reach as high as 10^4 in some cases we studied, whereas with Lasso regression, it can be reduced to less than 5 while the MSE only increases slightly. As previously discussed, this reduction in the ℓ_1 norm implies that the computational cost of the QEM protocol will decrease by orders of magnitude. Another advantage of Lasso regression is its tendency to set many coefficients to zero, meaning that in practical applications, we can omit constructing neighboring circuits of the target circuit for those coefficients that vanish.

B Optimality of the 2-Design Training Method

The mathematical properties of the 2-design training method are analyzed below. Specifically, we will prove that the function `combine` obtained by the linear regression or the Lasso regression based

on the training set generated by 2-training method is, in some sense, optimal among all linear functions as $T \rightarrow \infty$. To achieve this, we first define a concept called “*quantum rotation t -design*” and show that the gate set produced in 2-training method forms a quantum rotation 2-design. Then, we will prove that only $\mathcal{O}(\ln(N/\delta)/\varepsilon^2)$ training circuits are needed to obtain a solution within ε distance from the optimal linear solution with probability at least $1 - \delta$, where N is the number of neighbor circuits. Lastly, we will argue that achieving a small MSE on the training set guarantees that the worst-case error on the test set remains small with high probability.

B.1 Quantum Rotation t -design

Let $R_{\hat{n}}(\theta) := \exp(-i\theta\hat{n} \cdot \vec{\sigma}/2)$, where $\hat{n} = (n_x, n_y, n_z)$ is a unit vector and $\vec{\sigma} = (X, Y, Z)$. It is not hard to see that the set $\mathcal{G}_{\hat{n}} := \{R_{\hat{n}}(\theta)\}_{\theta \in [0, 2\pi]}$ forms a group, which is a subgroup of the single-qubit unitary group $U(2)$. Similar to unitary t -design [45], here we consider the t -design over the group $\mathcal{G}_{\hat{n}}$, which we call the *quantum rotation t -design*.

Definition 3. A set of unitary matrices $\{A_i\}_{i=1}^K$ on $\mathbb{C}^{2 \times 2}$ is called a *quantum rotation t -design* with respect to $R_{\hat{n}}(\theta)$, if

$$\frac{1}{K} \sum_{i=1}^K \left(A_i \otimes A_i^\dagger \right)^{\otimes t} = \frac{1}{2\pi} \int_0^{2\pi} (R_{\hat{n}}(\theta) \otimes R_{\hat{n}}(-\theta))^{\otimes t} d\theta.$$

We now prove that the gate set utilized in 2-training method actually forms a quantum rotation 2-design.

Theorem 4. $\{R_{\hat{n}}(\theta)\}_{\theta=0, \pi/2, \pi, 3\pi/2}$ is a quantum rotation 2-design with respect to $\{R_{\hat{n}}(\theta)\}_{\theta \in [0, 2\pi]}$.

Proof. Define the matrix M as $M = \hat{n} \cdot \vec{\sigma}$, and then $R_{\hat{n}}(\theta) = \exp(-i\theta M/2)$. Using the relations

$$\begin{aligned} \frac{1}{2\pi} \int_0^{2\pi} \cos^4 \frac{\theta}{2} d\theta &= \frac{1}{2\pi} \int_0^{2\pi} \sin^4 \frac{\theta}{2} d\theta = \frac{3}{8}, \\ \frac{1}{2\pi} \int_0^{2\pi} \cos \frac{\theta}{2} \sin^3 \frac{\theta}{2} d\theta &= \frac{1}{2\pi} \int_0^{2\pi} \cos^3 \frac{\theta}{2} \sin \frac{\theta}{2} d\theta = 0, \\ \frac{1}{2\pi} \int_0^{2\pi} \cos^2 \frac{\theta}{2} \sin^2 \frac{\theta}{2} d\theta &= \frac{1}{8}, \end{aligned}$$

we have

$$\begin{aligned} &\frac{1}{2\pi} \int_0^{2\pi} R_{\hat{n}}(\theta)^{\otimes 2} \otimes R_{\hat{n}}(-\theta)^{\otimes 2} d\theta \\ &= \sum_{i_1, \dots, i_4=0}^1 \frac{1}{2\pi} \int_0^{2\pi} i^{-i_1-i_2+i_3+i_4} \left(\cos \frac{\theta}{2} \right)^{4-\sum_j i_j} \times \\ &\quad \left(\sin \frac{\theta}{2} \right)^{\sum_j i_j} \times \left(\bigotimes_{j=1}^4 M^{i_j} \right) d\theta \\ &= \frac{3}{8} I^{\otimes 4} + \frac{3}{8} M^{\otimes 4} + \frac{1}{8} \sum_{\substack{i_1, \dots, i_4=0 \\ i_1+\dots+i_4=2}}^1 i^{-i_1-i_2+i_3+i_4} \bigotimes_{j=1}^4 M^{i_j}. \end{aligned}$$

Meanwhile, it can be verified that

$$\begin{aligned}
& \frac{1}{4} \sum_{k=0}^3 R_{\hat{n}} \left(\frac{k\pi}{2} \right)^{\otimes 2} \otimes R_{\hat{n}} \left(\frac{-k\pi}{2} \right)^{\otimes 2} \\
&= \frac{1}{4} \left(1 + \frac{1}{4} + \frac{1}{4} \right) I^{\otimes 4} + \frac{1}{4} \left(1 + \frac{1}{4} + \frac{1}{4} \right) M^{\otimes 4} \\
&+ \frac{1}{4} \left(\frac{1}{4} + \frac{1}{4} \right) \sum_{\substack{i_1, \dots, i_4=0 \\ i_1 + \dots + i_4=2}}^1 i^{-i_1-i_2+i_3+i_4} \bigotimes_{j=1}^4 M^{i_j} \\
&= \frac{3}{8} I^{\otimes 4} + \frac{3}{8} M^{\otimes 4} + \frac{1}{8} \sum_{\substack{i_1, \dots, i_4=0 \\ i_1 + \dots + i_4=2}}^1 i^{-i_1-i_2+i_3+i_4} \bigotimes_{j=1}^4 M^{i_j},
\end{aligned}$$

which concludes the proof. \square

Now we are ready to prove the optimality of the solutions obtained by linear regression and Lasso regression on the training circuits generated by 2-training method.

B.2 Asymptotic Optimality

We prove that under the 2-design training method, both linear regression and Lasso regression achieve optimal solutions on the training set as its size T approaches infinity. Interestingly, these solutions coincide with the optimal solutions on the test set on average. This demonstrates the strong generalization capability of the 2-design training method. We first analyze the idealized setting without quantum measurement shot noise, then extend our proof to account for shot noise effects.

B.2.1 Optimality without Shot Noise

Firstly, recall that the training set is

$$\mathbb{S} = \left\{ \left(\left(x_1^{(i)}, \dots, x_N^{(i)} \right)^\top, y^{(i)} \right) \right\}_{i=1, \dots, T},$$

where the feature vector $\mathbf{x}^{(i)} = (x_1^{(i)}, \dots, x_N^{(i)})^\top$ records the noisy expectation values for the N neighbor circuits of the i -th training circuit $C^{(i)}$, $y^{(i)}$ represents the ideal expectation value for this training circuit, and T is the number of training circuits. We denote by $P_{\mathbb{S}}$ the underlying probability distribution of the training circuit $C^{(i)}$, which is determined by how we generate the training set \mathbb{S} , i.e., how the single-qubit Pauli rotation gates are replaced by Clifford gates. In the 2-design training method, the rotation angles of the Pauli gates are randomly reset to one of four distinct values.

With a slight abuse of notation, we also denote $P_{\mathbb{S}}$ as the probability distribution of all types of data generated from the training circuit $C^{(i)}$, for example, the feature vector $\mathbf{x}^{(i)}$ and the label $y^{(i)}$. Similarly, we define P_{test} as the underlying distribution of the target circuit, where all parameters in the parameterized circuits are sampled uniformly in $[0, 2\pi)$.

Linear regression. The goal of a linear regression model is to learn a linear function such that, for each training circuit, it can simultaneously map the N noisy expectation values from neighbor circuits to the ideal expectation value, i.e., the mapping has the form $\hat{y} = \sum_{j=1}^N c_j x_j$, where c_j 's are the parameters we need to learn. For this, we aim to minimize the average MSE on the training set

$$\min_{c_1, \dots, c_N} \frac{1}{T} \sum_{i=1}^T \left(\sum_{j=1}^N c_j x_j^{(i)} - y^{(i)} \right)^2.$$

When the size of the training set tends to infinity, i.e., $T \rightarrow \infty$, the solution we obtained is actually the solution to the following optimization problem:

$$\min_{c_1, \dots, c_N} \mathbb{E}_{((x_1, \dots, x_N), y) \sim P_S} \left(\sum_{j=1}^N c_j x_j - y \right)^2. \quad (8)$$

We now formulate Eq. (8) as a quadratic programming problem. Define $\mathbf{c} := (c_1, c_2, \dots, c_N)^\top$, $\mathbf{x} := (x_1, x_2, \dots, x_N)^\top$, then Eq. (8) can be rewritten as

$$\begin{aligned} & \min_{\mathbf{c}} \mathbb{E}_{(\mathbf{x}, y) \sim P_S} (\mathbf{c}^\top \mathbf{x} - y)^2 \\ &= \min_{\mathbf{c}} \mathbb{E}_{(\mathbf{x}, y) \sim P_S} (\mathbf{c}^\top \mathbf{x} - y) (\mathbf{c}^\top \mathbf{x} - y)^\top \\ &= \min_{\mathbf{c}} \mathbf{c}^\top \mathbb{E}_{(\mathbf{x}, y) \sim P_S} [\mathbf{x} \mathbf{x}^\top] \mathbf{c} - 2\mathbf{c}^\top \mathbb{E}_{(\mathbf{x}, y) \sim P_S} [\mathbf{y} \mathbf{x}] + \mathbb{E}_{(\mathbf{x}, y) \sim P_S} y^2. \end{aligned}$$

Since the coefficient matrix $\mathbb{E}_{(\mathbf{x}, y) \sim P_S} [\mathbf{x} \mathbf{x}^\top]$ is positive semidefinite, Eq. (8) is a quadratic programming problem with a semidefinite coefficient matrix [49], whose solution is given by

$$\mathbf{c}^* = \begin{pmatrix} \mathbb{E}_{P_S} x_1 x_1 & \cdots & \mathbb{E}_{P_S} x_1 x_N \\ \vdots & \ddots & \vdots \\ \mathbb{E}_{P_S} x_N x_1 & \cdots & \mathbb{E}_{P_S} x_N x_N \end{pmatrix}^{-1} \begin{pmatrix} \mathbb{E}_{P_S} x_1 y \\ \vdots \\ \mathbb{E}_{P_S} x_N y \end{pmatrix}, \quad (9)$$

where we write $\mathbb{E}_{(\mathbf{x}, y) \sim P_S}$ as \mathbb{E}_{P_S} for simplicity. If $\mathbb{E}_{(\mathbf{x}, y) \sim P_S} [\mathbf{x} \mathbf{x}^\top]$ is not invertible, then the pseudoinverse should be used instead [50]. For the convenience of later discussion, we introduce the following notations:

$$\mathbf{A} = \begin{pmatrix} x_1 x_1 & \cdots & x_1 x_N \\ \vdots & \ddots & \vdots \\ x_N x_1 & \cdots & x_N x_N \end{pmatrix}, \quad \mathbf{a} = \begin{pmatrix} x_1 y \\ \vdots \\ x_N y \end{pmatrix}. \quad (10)$$

Then Eq. (9) becomes $\mathbf{c}^* = \begin{pmatrix} \mathbb{E}[\mathbf{A}] \\ \mathbb{E}[\mathbf{a}] \end{pmatrix}^{-1} \mathbb{E}[\mathbf{a}]$.

After training, we hope that the obtained model can effectively mitigate errors in the target parameterized quantum circuits. Next, we show that using 2-training method to construct the training set, the optimal solution \mathbf{c}^* obtained on the training set is also an optimal solution on the test set.

To see this, we first estimate the smallest average MSE that a linear model can possibly achieve on the target parameterized quantum circuits, which is the solution to the optimization problem

$$\min_{\mathbf{c}} \mathbb{E}_{(\mathbf{x}, y) \sim P_{\text{test}}} (\mathbf{c}^\top \mathbf{x} - y)^2, \quad (11)$$

where P_{test} is the underlying distribution of the test dataset. Here, each data point also includes the noisy expectation values of all the neighbor circuits and the noiseless expectation value of the target circuit. Then the solution to Eq. (11) is actually

$$\begin{pmatrix} \mathbb{E}_{P_{\text{test}}} x_1 x_1 & \cdots & \mathbb{E}_{P_{\text{test}}} x_1 x_N \\ \vdots & \ddots & \vdots \\ \mathbb{E}_{P_{\text{test}}} x_N x_1 & \cdots & \mathbb{E}_{P_{\text{test}}} x_N x_N \end{pmatrix}^{-1} \begin{pmatrix} \mathbb{E}_{P_{\text{test}}} x_1 y \\ \vdots \\ \mathbb{E}_{P_{\text{test}}} x_N y \end{pmatrix}, \quad (12)$$

which can also be written as $\begin{pmatrix} \mathbb{E}_{P_{\text{test}}} [\mathbf{A}] \\ \mathbb{E}_{P_{\text{test}}} [\mathbf{a}] \end{pmatrix}^{-1} \mathbb{E}_{P_{\text{test}}} [\mathbf{a}]$. Here, we have used the shorthand notation $\mathbb{E}_{P_{\text{test}}}$ for $\mathbb{E}_{(\mathbf{x}, y) \sim P_{\text{test}}}$.

The following lemma builds a key connection between the data of computing produced by the training circuits and that by the target circuits.

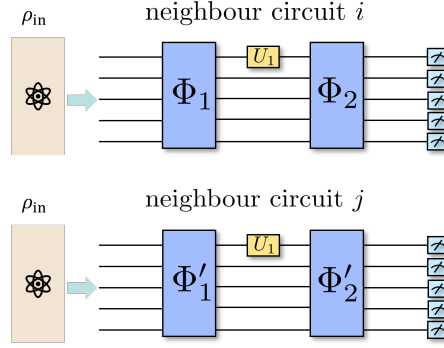


Figure 7: The i -th and the j -th neighbor circuits

Lemma 1. Suppose the training circuits are generated by 2-training method. If we apply the same neighbor map to the training circuits and the target quantum circuit, we will have that $\mathbb{E}[\mathbf{A}] = \mathbb{E}_{P_{\text{test}}}[\mathbf{A}]$, $\mathbb{E}[\mathbf{a}] = \mathbb{E}_{P_{\text{test}}}[\mathbf{a}]$, and $\mathbb{E}[y^2] = \mathbb{E}_{P_{\text{test}}}[y^2]$.

Proof. Assume that U_1 is a single-qubit gate acting on the first qubit of neighbor circuits, and the corresponding rotation angle is θ_1 . Let Φ_1 (Φ'_1) denote the noisy channel corresponding to the operations of all the gates before U_1 in the i -th (j -th) neighbor circuit. Define $\rho = \Phi_1(\rho_{\text{in}})$ and $\rho' = \Phi'_1(\rho_{\text{in}})$, where ρ_{in} is the same input state of all the circuits. Similarly, let Φ_2 (Φ'_2) be the channel corresponding to the operations of all the gates after U_1 in the i -th (j -th) neighbor circuit. See Fig. 7 for an illustration.

Suppose $U_1 = R_{\hat{n}}(\theta_1) = \exp(-i\theta_1 M/2)$, where $M = \hat{n} \cdot \vec{\sigma}$. Then

$$\begin{aligned} & \mathbb{E}_{U_1} \text{tr} \left(\left(U_1 \rho U_1^\dagger \right) \Phi_2^\dagger(O) \right) \text{tr} \left(\left(U_1 \rho' U_1^\dagger \right) \Phi_2'^\dagger(O) \right) \\ &= \mathbb{E}_{\theta_1 \in [0, 2\pi]} \text{tr} \left(\left(R_{\hat{n}}(\theta_1) \rho R_{\hat{n}}(-\theta_1) \right) \Phi_2^\dagger(O) \right) \text{tr} \left(\left(R_{\hat{n}}(\theta_1) \rho' R_{\hat{n}}(-\theta_1) \right) \Phi_2'^\dagger(O) \right) \\ &= \mathbb{E}_{\theta_1 \in \{0, \frac{\pi}{2}, \pi, \frac{3}{2}\pi\}} \text{tr} \left(\left(R_{\hat{n}}(\theta_1) \rho R_{\hat{n}}(-\theta_1) \right) \Phi_2^\dagger(O) \right) \text{tr} \left(\left(R_{\hat{n}}(\theta_1) \rho' R_{\hat{n}}(-\theta_1) \right) \Phi_2'^\dagger(O) \right), \end{aligned}$$

where the last equality holds because $\{R_{\hat{n}}(\theta_1)\}_{\theta_1=0,\pi/2,\pi,3\pi/2}$ forms a quantum rotation 2-design. Suppose all the other parameterized gates in the circuits are U_2, U_3, \dots, U_M with the corresponding rotation angles $\theta_2, \theta_3, \dots, \theta_M$, which are contained in Φ_2 and Φ'_2 . It follows that

$$\begin{aligned} & \mathbb{E}_{P_{\text{test}}} x_i x_j = \mathbb{E}_{U_M} \cdots \mathbb{E}_{U_1} x_i x_j \\ &= \mathbb{E}_{\theta_1, \dots, \theta_M \in [0, 2\pi]} \text{tr} \left(\left(R_{\hat{n}}(\theta_1) \rho R_{\hat{n}}(-\theta_1) \right) \Phi_2^\dagger(O) \right) \text{tr} \left(\left(R_{\hat{n}}(\theta_1) \rho' R_{\hat{n}}(-\theta_1) \right) \Phi_2'^\dagger(O) \right) \\ &= \mathbb{E}_{\theta_2, \dots, \theta_M \in [0, 2\pi]} \text{tr} \left(\left(R_{\hat{n}}(\theta_1) \rho R_{\hat{n}}(-\theta_1) \right) \Phi_2^\dagger(O) \right) \text{tr} \left(\left(R_{\hat{n}}(\theta_1) \rho' R_{\hat{n}}(-\theta_1) \right) \Phi_2'^\dagger(O) \right) \\ &= \mathbb{E}_{\theta_2, \dots, \theta_M \in [0, 2\pi]} x_i x_j. \end{aligned}$$

We conclude the proof by repeating the above procedure for $\theta_2, \theta_3, \dots, \theta_M$ sequentially. \square

Together with Eq. (9) and Eq. (12), Lemma 1 leads to the following conclusion.

Theorem 5 (Optimality, linear regression). *Suppose the training set*

$$\mathbb{S} = \left\{ \left(\left(x_1^{(i)}, \dots, x_N^{(i)} \right)^\top, y^{(i)} \right) \right\}_{i=1, \dots, T}$$

is produced by 2-training method. Then the solution obtained from the linear regression in Eq. (6) is also a solution to the linear regression Eq. (11) on the target circuit when $T \rightarrow \infty$.

Lasso regression. Recall that to reduce the computational cost of learning-based QEM, one can replace linear regression with Lasso regression to fit the training data. Below, as a counterpart to Theorem 5, we prove that 2-training method also enables Lasso regression to achieve optimal solutions on both the training set and test set.

Theorem 6 (Optimality, Lasso regression). *The solution to the Lasso regression on the training circuit set generated by 2-training method is also a solution for the target parameterized circuits as the size of the training set $T \rightarrow \infty$.*

Proof. Recall that the optimization problem that the Lasso regression tries to solve on the training set is

$$\begin{aligned} & \min_{c_1, \dots, c_N} \frac{1}{T} \sum_{i=1}^T \left(\sum_{j=1}^N c_j x_j^{(i)} - y^{(i)} \right)^2 \\ & \text{subject to } \sum_i |c_i| \leq \gamma. \end{aligned} \quad (13)$$

When $T \rightarrow \infty$, the above problem can also be written as the following optimization problem:

$$\begin{aligned} & \min_{\mathbf{c}} \mathbf{c}^\top \mathbb{E}_{P_{\text{S}}} [\mathbf{A}] \mathbf{c} - 2\mathbf{c}^\top \mathbb{E}_{P_{\text{S}}} [\mathbf{a}] + \mathbb{E}_{P_{\text{S}}} y^2 \\ & \text{subject to } \|\mathbf{c}\|_1 \leq \gamma. \end{aligned}$$

According to Lemma 1, its solution is also the solution to the following optimization problem:

$$\begin{aligned} & \min_{\mathbf{c}} \mathbf{c}^\top \mathbb{E}_{P_{\text{test}}} [\mathbf{A}] \mathbf{c} - 2\mathbf{c}^\top \mathbb{E}_{P_{\text{test}}} [\mathbf{a}] + \mathbb{E}_{P_{\text{test}}} y^2 \\ & \text{subject to } \|\mathbf{c}\|_1 \leq \gamma, \end{aligned}$$

which is exactly the Lasso regression on the target parameterized circuit. \square

B.2.2 Optimality with Shot Noise

In this subsection, we discuss the impact of shot noise on our protocol. Previously, we have proven that our method yields the optimal linear solutions if we apply either linear regression or Lasso regression on a training set generated by 2-training method, where the noisy expectation values obtained are exact. However, in practice, all the noisy expectation values in the feature vectors are obtained by quantum measurements, which introduce statistical errors for each expectation value $x_j^{(i)}$ defined in Eq. (3). Specifically, if we measure each neighbor circuit N_s times and average the outcomes to get the expectation value, the actual training set takes the following form:

$$\mathbb{S}^{N_s} = \left\{ \left(\mathbf{x}_{N_s}^{(i)}, y^{(i)} \right) \right\}_{i \in [T]}, \quad (14)$$

where $\mathbf{x}_{N_s}^{(i)}$ denotes the feature vector of the i -th training circuit. The j -th element of $\mathbf{x}_{N_s}^{(i)}$ is

$$\left(\mathbf{x}_{N_s}^{(i)} \right)_j = \frac{1}{N_s} \sum_{k=1}^{N_s} x_{j,k}^{(i)}, \quad (15)$$

where $x_{j,k}^{(i)}$ denotes the k -th measurement outcome on the j -th neighbor circuit of the i -th training circuit. As N_s increases, we have $\mathbf{x}^{(i)} = \lim_{N_s \rightarrow \infty} \mathbf{x}_{N_s}^{(i)}$.

We now prove that the linear (Lasso) regression problem defined in Eq. (6) (Eq. (7)) on the training set \mathbb{S}^{N_s} is equivalent to the linear (Lasso) regression problem with an additional ℓ_2 regularization term defined on the test dataset [51], when $T \rightarrow \infty$. In particular, the strength of this regularization term is inversely proportional to N_s . In many linear regression protocols, an ℓ_2 regularization term is added to avoid overfitting [52] and improve numerical stability [51, 53]. Interestingly, in our task, shot noise naturally introduces an ℓ_2 penalty term, making the optimization problem more stable and easier to solve.

To prove this statement, we require the following lemma, which establishes the relationship between the average variance of the measurement outcomes on the training set and that on the test set.

Lemma 2. *Let C be randomly sampled from the test circuits and let $C^{(i)}$ be a training circuit generated by the 2-design method (2-training method). Apply the same neighbor map to C and $C^{(i)}$ to obtain the corresponding neighbor circuits (C_1, \dots, C_N) and $(C_1^{(i)}, \dots, C_N^{(i)})$, respectively. Denote by $x_{j,1}^{(i)}$ and $o_{j,1}$ the measurement outcomes of measuring the observable O on the j -th neighbor circuit of $C^{(i)}$ and C , respectively. Then, we have*

$$\mathbb{E}_{P_{\text{S}}} [\text{Var}[x_{j,1}^{(i)}]] = \mathbb{E}_{P_{\text{test}}} [\text{Var}[o_{j,1}]]$$

for any $j \in [N]$, where the randomness of Var is from quantum measurements.

Proof. The proof technique is similar to that in the proof for Lemma 1. Suppose that the noisy output state of the j -th neighbor circuit of $C^{(i)}$ is ρ . Then we have

$$\text{Var}[x_{j,1}^{(i)}] = \text{tr}(\rho O^2) - \text{tr}(\rho O)^2.$$

As in the proof for Lemma 1, we examine $\mathbb{E}_{P_{\text{S}}} [\text{Var}[x_{j,1}^{(i)}]]$ gate by gate. Suppose that $\rho = \Phi_2(R_{\hat{n}}(\theta_1) \Phi_1(\rho_{\text{in}}) R_{\hat{n}}(-\theta_1))$, where ρ_{in} , $R_{\hat{n}}(\theta_1)$, and Φ_i ($i = 1, 2$) are defined similarly as in Lemma 1. Then it holds that

$$\begin{aligned} & \mathbb{E}_{\theta_1 \in \{0, \frac{\pi}{2}, \pi, \frac{3}{2}\pi\}} \text{tr}(\rho O^2) \\ &= \mathbb{E}_{\theta_1 \in \{0, \frac{\pi}{2}, \pi, \frac{3}{2}\pi\}} \text{tr} \left((R_{\hat{n}}(\theta_1) \Phi_1(\rho_{\text{in}}) R_{\hat{n}}(-\theta_1)) \Phi_2^\dagger(O^2) \right) \\ &= \mathbb{E}_{\theta_1 \in [0, 2\pi]} \text{tr} \left((R_{\hat{n}}(\theta_1) \Phi_1(\rho_{\text{in}}) R_{\hat{n}}(-\theta_1)) \Phi_2^\dagger(O^2) \right), \end{aligned}$$

where the last equality holds because $\{R_{\hat{n}}(\theta)\}_{\theta=0,\pi/2,\pi,3\pi/2}$ is a quantum rotation 2-design, implying that it is also a quantum rotation 1-design. Taking the expectation over all random rotation gates, denoted as U_1, \dots, U_M , we obtain that

$$\begin{aligned} \mathbb{E}_{P_{\text{S}}} \text{tr}(\rho O^2) &= \mathbb{E}_{U_M} \cdots \mathbb{E}_{U_1} \text{tr}(\rho O^2) \\ &= \mathbb{E}_{\theta_1, \dots, \theta_M \in \{0, \frac{\pi}{2}, \pi, \frac{3}{2}\pi\}} \text{tr} \left((R_{\hat{n}}(\theta_1) \Phi_1(\rho_{\text{in}}) R_{\hat{n}}(-\theta_1)) \Phi_2^\dagger(O^2) \right) \\ &= \mathbb{E}_{\substack{\theta_1 \in [0, 2\pi] \\ \theta_2, \dots, \theta_M \in \{0, \frac{\pi}{2}, \pi, \frac{3}{2}\pi\}}} \text{tr} \left((R_{\hat{n}}(\theta_1) \Phi_1(\rho_{\text{in}}) R_{\hat{n}}(-\theta_1)) \Phi_2^\dagger(O^2) \right), \end{aligned}$$

where the parameters $\theta_2, \dots, \theta_M$ are contained in Φ_2 . Repeating the above procedure for U_2, \dots, U_M sequentially yields that

$$\begin{aligned} \mathbb{E}_{P_{\text{S}}} \text{tr}(\rho O^2) &= \mathbb{E}_{U_M} \cdots \mathbb{E}_{U_1} \text{tr}(\rho O^2) \\ &= \mathbb{E}_{\theta_1, \dots, \theta_M \in [0, 2\pi]} \text{tr} \left((R_{\hat{n}}(\theta_1) \Phi_1(\rho_{\text{in}}) R_{\hat{n}}(-\theta_1)) \Phi_2^\dagger(O^2) \right) \\ &= \mathbb{E}_{P_{\text{test}}} \text{tr} \left((R_{\hat{n}}(\theta_1) \Phi_1(\rho_{\text{in}}) R_{\hat{n}}(-\theta_1)) \Phi_2^\dagger(O^2) \right) \\ &= \mathbb{E}_{P_{\text{test}}} \text{tr}(\rho' O^2), \end{aligned}$$

where we denoted the output state of the j -th neighbor of the target circuit as ρ' . According to

Lemma 1, we know that $\mathbb{E}_{P_S} \text{tr}(\rho O)^2 = \mathbb{E}_{P_{\text{test}}} \text{tr}(\rho' O)^2$. Putting them together, we have

$$\begin{aligned} \mathbb{E}_{P_S} [\text{Var}[x_{j,1}^{(i)}]] &= \mathbb{E}_{P_S} [\text{tr}(\rho O^2) - \text{tr}(\rho O)^2] \\ &= \mathbb{E}_{P_{\text{test}}} [\text{tr}(\rho' O^2) - \text{tr}(\rho' O)^2] \\ &= \mathbb{E}_{P_{\text{test}}} [\text{Var}[o_{j,1}]]. \end{aligned}$$

□

Now we are ready to prove the asymptotic optimality of the 2-design training method in the presence of shot noise. Specifically, we will show that the shot noise introduces an additional ℓ_2 regularization term to the optimization problem we need to address. Recall that

$$\mathbf{A} = \mathbf{x}\mathbf{x}^\top, \quad \mathbf{a} = \begin{pmatrix} x_1 y \\ \vdots \\ x_N y \end{pmatrix},$$

where $\mathbf{x} = (x_1, \dots, x_N)^\top$. For linear regression, we have the following theorem.

Theorem 7. *Consider the training dataset*

$$\mathbb{S}^{N_s} = \left\{ \left(\left(\frac{1}{N_s} \sum_{j=1}^{N_s} x_{1,j}^{(i)}, \dots, \frac{1}{N_s} \sum_{j=1}^{N_s} x_{N,j}^{(i)} \right)^\top, y^{(i)} \right) \right\}_{i \in [T]},$$

where the training circuits are generated with 2-training method. When $T \rightarrow \infty$, the solution obtained from the linear regression problem in Eq. (6) is also a solution to the following regression problem on the target circuit:

$$\min_{\mathbf{c}} \mathbf{c}^\top \mathbb{E}_{P_{\text{test}}} [\mathbf{A} + \mathbf{\Lambda}_{N_s}] \mathbf{c} - 2 \mathbb{E}_{P_{\text{test}}} [\mathbf{a}]^\top \mathbf{c} + \mathbb{E}_{P_{\text{test}}} y^2,$$

The matrix $\mathbf{\Lambda}_{N_s}$ is defined as

$$\mathbf{\Lambda}_{N_s} := \frac{\text{diag}(X_1, \dots, X_N)}{N_s},$$

where X_i is the variance of observable O associated with the i -th neighbor circuit of the target circuit.

Proof. We first introduce some random variables $\varepsilon_{i,j}$'s to represent the shot noise caused by quantum measurements. Specifically, we define

$$\varepsilon_{i,j} := \frac{1}{N_s} \sum_{k=1}^{N_s} x_{j,k}^{(i)} - x_j^{(i)},$$

for $i \in [T]$ and $j \in [N]$.

Next, we investigate the statistical properties of $\varepsilon_{i,j}$. Denote $\mathbb{E}_{\mathcal{M}}$ as the expectation with respect to the measurement outcomes. Then, conditioned on the training circuit $C^{(i)}$ being sampled, we have

$$\mathbb{E}_{\mathcal{M}} [\varepsilon_{i,j} | C^{(i)}] = \frac{1}{N_s} \sum_{k=1}^{N_s} x_j^{(i)} - x_j^{(i)} = 0.$$

Similarly, we compute its second moment:

$$\begin{aligned}
& \mathbb{E}_{\mathcal{M}}[\varepsilon_{i,j}^2 | C^{(i)}] \\
&= \mathbb{E}_{\mathcal{M}} \left[\frac{1}{N_s^2} \left(\sum_{k=1}^{N_s} (x_{j,k}^{(i)})^2 + \sum_{k_1 \neq k_2} x_{j,k_1}^{(i)} x_{j,k_2}^{(i)} \right) - \frac{2x_j^{(i)}}{N_s} \sum_k x_{j,k}^{(i)} + (x_j^{(i)})^2 \middle| C^{(i)} \right] \\
&= \mathbb{E}_{\mathcal{M}} \left[\frac{1}{N_s^2} \sum_{k=1}^{N_s} (x_{j,k}^{(i)})^2 \middle| C^{(i)} \right] + \frac{(N_s - 1)}{N_s} (x_j^{(i)})^2 - (x_j^{(i)})^2 \\
&= \mathbb{E}_{\mathcal{M}} \left[\frac{1}{N_s} (x_{j,1}^{(i)})^2 \middle| C^{(i)} \right] - \frac{1}{N_s} (x_j^{(i)})^2 \\
&= \frac{1}{N_s} \text{Var}[x_{j,1}^{(i)}].
\end{aligned}$$

Here, the penultimate equality holds because $x_{j,k}^{(i)}$ is sampled from the same probability distribution independently for any $k \in [N_s]$. We now rewrite the feature vector of the i -th training circuit as

$$\begin{aligned}
\mathbf{x}_{N_s}^{(i)} &= \left(\frac{1}{N_s} \sum_{j=1}^{N_s} x_{1,j}^{(i)}, \dots, \frac{1}{N_s} \sum_{j=1}^{N_s} x_{N_s,j}^{(i)} \right)^\top \\
&= (x_1^{(i)} + \varepsilon_{i,1}, \dots, x_N^{(i)} + \varepsilon_{i,N})^\top.
\end{aligned}$$

Then, the linear regression defined on the training set \mathbb{S}^{N_s} can be expressed as

$$\begin{aligned}
& \min_{\mathbf{c}} \frac{1}{T} \sum_{i=1}^T \left(\mathbf{c}^\top \mathbf{x}_{N_s}^{(i)} - y^{(i)} \right)^2 \\
&= \min_{\mathbf{c}} \mathbf{c}^\top \left(\frac{1}{T} \sum_{i=1}^T \mathbf{x}_{N_s}^{(i)} \mathbf{x}_{N_s}^{(i)\top} \right) \mathbf{c} - 2 \frac{1}{T} \sum_{i=1}^T y^{(i)} \mathbf{x}_{N_s}^{(i)\top} \mathbf{c} + \frac{1}{T} \sum_{i=1}^T (y^{(i)})^2.
\end{aligned}$$

Treat $\mathbf{x}_{N_s}^{(i)} \mathbf{x}_{N_s}^{(i)\top}$, $y^{(i)} \mathbf{x}_{N_s}^{(i)\top}$ and $(y^{(i)})^2$ as random variables. Then, as $T \rightarrow \infty$, the linear regression defined on training set \mathbb{S}^{N_s} reads

$$\min_{\mathbf{c}} \mathbf{c}^\top \mathbb{E}_{\text{train}} \left[\mathbf{x}_{N_s}^{(i)} \mathbf{x}_{N_s}^{(i)\top} \right] \mathbf{c} - 2 \mathbb{E}_{\text{train}} [y^{(i)} \mathbf{x}_{N_s}^{(i)\top}]^\top \mathbf{c} + \mathbb{E}_{\text{train}} \left[(y^{(i)})^2 \right],$$

where the expectation $\mathbb{E}_{\text{train}} := \mathbb{E}_{P_{\mathbb{S}} \mathcal{M}}$ is taken over two sources of randomness, namely, the probability distribution of the training data point $P_{\mathbb{S}}$ and quantum measurements.

Next, we compute $\mathbb{E}_{\text{train}} \left[\mathbf{x}_{N_s}^{(i)} \mathbf{x}_{N_s}^{(i)\top} \right]$, $\mathbb{E}_{\text{train}} [y^{(i)} \mathbf{x}_{N_s}^{(i)\top}]^\top$ and $\mathbb{E}_{\text{train}} \left[(y^{(i)})^2 \right]$. Based on this observation and the law of total expectation, we have that when $j \neq k$,

$$\begin{aligned}
& \left(\mathbb{E}_{\text{train}} \left[\mathbf{x}_{N_s}^{(i)} \mathbf{x}_{N_s}^{(i)\top} \right] \right)_{j,k} \\
&= \mathbb{E}_{P_{\mathbb{S}}} \left[\mathbb{E}_{\mathcal{M}} \left[(x_j^{(i)} + \varepsilon_{i,j}) (x_k^{(i)} + \varepsilon_{i,k}) \middle| C^{(i)} \right] \right] \\
&= \mathbb{E}_{P_{\mathbb{S}}} [x_j^{(i)} x_k^{(i)}] = \mathbb{E}_{P_{\text{test}}} [x_j x_k],
\end{aligned}$$

The diagonal elements of this matrix is given by

$$\begin{aligned}
& \left(\mathbb{E}_{\text{train}} \left[\mathbf{x}_{N_s}^{(i)} \mathbf{x}_{N_s}^{(i)\top} \right] \right)_{j,j} \\
&= \mathbb{E}_{P_{\mathbb{S}}} \left[\mathbb{E}_{\mathcal{M}} \left[(x_j^{(i)} + \varepsilon_{i,j})^2 \middle| C^{(i)} \right] \right] \\
&= \mathbb{E}_{P_{\mathbb{S}}} \left[(x_j^{(i)})^2 \right] + \mathbb{E}_{P_{\mathbb{S}}} \left[\text{Var}[x_{j,1}^{(i)}] \right] / N_s,
\end{aligned}$$

where $j \in [N]$ and the last equality holds because $\mathbb{E}_{\mathcal{M}}[\varepsilon_{i,j}^2] = \frac{1}{N_s} \text{Var}[x_{j,1}^{(i)}]$. According to Lemma 1 and Lemma 2, we have that $\mathbb{E}_{P_S} \left[\left(x_j^{(i)} \right)^2 \right] = \mathbb{E}_{P_{\text{test}}} [x_j^2]$ and $\mathbb{E}_{P_S} \left[\text{Var}[x_{j,1}^{(i)}] \right] = \mathbb{E}_{P_{\text{test}}} [X_j]$, where $X_j := \text{Var}[o_{j,1}]$ is the variance of the measurement outcomes for the j -th neighbor circuit of the target circuit. Then, we have

$$\left(\mathbb{E}_{\text{train}} \left[\mathbf{x}_{N_s}^{(i)} \mathbf{x}_{N_s}^{(i)\top} \right] \right)_{j,j} = \mathbb{E}_{P_{\text{test}}} [x_j^2] + \mathbb{E}_{P_{\text{test}}} [X_j]/N_s.$$

Therefore, it holds that

$$\mathbb{E}_{\text{train}} \left[\mathbf{x}_{N_s}^{(i)} \mathbf{x}_{N_s}^{(i)\top} \right] = \mathbb{E}_{P_{\text{test}}} [\mathbf{A} + \mathbf{\Lambda}_{N_s}],$$

where $\mathbf{\Lambda}_{N_s} := \frac{\text{diag}(X_1, \dots, X_N)}{N_s}$. Next we compute $\mathbb{E}_{\text{train}} [y^{(i)} \mathbf{x}_{N_s}^{(i)}]$:

$$\begin{aligned} & \left(\mathbb{E}_{\text{train}} [y^{(i)} \mathbf{x}_{N_s}^{(i)}] \right)_j \\ &= \mathbb{E}_{P_S} \left[\mathbb{E}_{\mathcal{M}} \left[y^{(i)} \left(x_j^{(i)} + \varepsilon_{i,j} \right) \middle| C^{(i)} \right] \right] \\ &= \mathbb{E}_{P_S} [y^{(i)} x_j^{(i)}] = \mathbb{E}_{P_{\text{test}}} [y x_j]. \end{aligned}$$

Since the labels of the training set \mathbb{S}^{N_s} are computed classically, the randomness of $(y^{(i)})^2$ only comes from the probability distribution of the training dataset P_S . Then we have

$$\mathbb{E}_{\text{train}} \left[\left(y^{(i)} \right)^2 \right] = \mathbb{E}_{P_S} \left[\left(y^{(i)} \right)^2 \right] = \mathbb{E}_{P_{\text{test}}} \left[\left(y^{(i)} \right)^2 \right],$$

where the last equality can be obtained directly from Lemma 1. Therefore, when T is sufficiently large, we have

$$\begin{aligned} & \frac{1}{T} \sum_{i=1}^T \mathbf{x}_{N_s}^{(i)} \mathbf{x}_{N_s}^{(i)\top} \rightarrow \mathbb{E}_{P_{\text{test}}} [\mathbf{A} + \mathbf{\Lambda}_{N_s}], \\ & \frac{1}{T} \sum_{i=1}^T y^{(i)} \mathbf{x}_{N_s}^{(i)\top} \rightarrow \mathbb{E}_{P_{\text{test}}} [\mathbf{a}]^\top, \\ & \frac{1}{T} \sum_{i=1}^T \left(y^{(i)} \right)^2 \rightarrow \mathbb{E}_{P_{\text{test}}} \left[\left(y^{(i)} \right)^2 \right]. \end{aligned}$$

To conclude, when $T \rightarrow \infty$, the solution to the linear regression defined on the training set \mathbb{S}^{N_s} is also a solution to the following regression problem on the target circuit:

$$\min_{\mathbf{c}} \mathbf{c}^\top \mathbb{E}_{P_{\text{test}}} [\mathbf{A} + \mathbf{\Lambda}_{N_s}] \mathbf{c} - 2 \mathbb{E}_{P_{\text{test}}} [\mathbf{a}]^\top \mathbf{c} + \mathbb{E}_{P_{\text{test}}} y^2. \quad (16)$$

□

As a direct corollary of Theorem 7, the solution to Eq. (16) is also a solution to the linear regression on the target circuit in the presence of shot noise, if we measure all the involved quantum circuits with the same number of shots N_s .

Corollary 1. *As the size of the training set $T \rightarrow \infty$, the solution to the linear (Lasso) regression on the training set \mathbb{S}^{N_s} generated by 2-training method is also a solution to the linear (Lasso) regression on the target circuit, where all the expectation values of the neighbor circuits are obtained through N_s measurement shots.*

Proof. We only give the proof for the case of the linear regression, and the case of the Lasso regression can be proved similarly.

Given the target circuit, we apply the neighbor map to generate the corresponding neighbor circuits and collect the feature data by performing measurements on each neighbor circuit for N_s times. Let

$$\mathbf{x}_{N_s} = \left(\frac{1}{N_s} \sum_{j=1}^{N_s} o_{1,j}, \dots, \frac{1}{N_s} \sum_{j=1}^{N_s} o_{N_s,j} \right)^\top$$

denote the feature vector for the target circuit, where $o_{i,j}$ is the outcome when measuring the observable O for the j -th time on the output of the i -th neighbor circuit. The linear regression problem defined on the test dataset is

$$\begin{aligned} & \min_{\mathbf{c}} \mathbb{E}_{\text{test}} (\mathbf{c}^\top \mathbf{x}_{N_s} - y)^2 \\ &= \min_{\mathbf{c}} \mathbf{c}^\top \mathbb{E}_{\text{test}} [\mathbf{x}_{N_s} \mathbf{x}_{N_s}^\top] \mathbf{c} - 2 \mathbb{E}_{\text{test}} [y \mathbf{x}_{N_s}]^\top \mathbf{c} + \mathbb{E}_{\text{test}} y^2, \end{aligned} \quad (17)$$

where the expectation $\mathbb{E}_{\text{test}} := \mathbb{E}_{P_{\text{test}} \mathcal{M}}$ is taken over the target circuits and the randomness of measurement outcomes. Following a similar procedure as in the proof of Theorem 7, we obtain

$$\begin{aligned} \mathbb{E}_{\text{test}} [\mathbf{x}_{N_s} \mathbf{x}_{N_s}^\top] &= \mathbb{E}_{P_{\text{test}}} [\mathbf{A} + \mathbf{\Lambda}_{N_s}], \\ \mathbb{E}_{\text{test}} [y \mathbf{x}_{N_s}] &= \mathbb{E}_{P_{\text{test}}} [\mathbf{a}]^\top. \end{aligned}$$

Therefore Eq. (17) can also be written as

$$\min_{\mathbf{c}} \mathbf{c}^\top \mathbb{E}_{P_{\text{test}}} [\mathbf{A} + \mathbf{\Lambda}_{N_s}] \mathbf{c} - 2 \mathbb{E}_{P_{\text{test}}} [\mathbf{a}]^\top \mathbf{c} + \mathbb{E}_{P_{\text{test}}} y^2,$$

which is identical to the linear regression defined on the training set when its size is sufficiently large. \square

From the above theorem and corollary, we observe that the ℓ_2 regularization term introduced by shot noise is given by

$$\mathbf{c}^\top \mathbb{E}_{P_{\text{test}}} [\mathbf{\Lambda}_{N_s}] \mathbf{c}.$$

It turns out that this regularization term helps us to achieve a better numerical stability, as the new coefficient matrix

$$\mathbb{E}_{P_{\text{test}}} [\mathbf{A} + \mathbf{\Lambda}_{N_s}]$$

would be less ill-conditioned. This suggests that shot noise helps the optimization process to converge more quickly. On the other hand, to ensure that the ℓ_2 regularization term does not dominate the obtained MSE, the norm of \mathbf{c} should not be too large. Otherwise, the required N_s will become excessively large, making the needed computational cost unacceptable.

C Estimation of the Computational Cost

C.1 Estimation of the Size of Training Set

We have argued that with a sufficiently large training set, our method is guaranteed to obtain the optimal linear solution with respect to the MSE. We now provide an estimate of how large is sufficient, and our conclusion suggests that the number of training circuits required is tolerable. Specifically, we will prove that only $\mathcal{O}(\ln(N/\delta)/\varepsilon^2)$ training circuits suffice to obtain a solution whose MSE is at most ε away from that of the case with no restrictions on the number of training circuits, with probability at least $1 - \delta$, where N is the number of neighbor circuits. In the following discussion, we treat the number of shots N_s used to estimate the expectation value of the observable O as a hyperparameter. Our proof holds for arbitrary N_s , including the case $N_s \rightarrow \infty$, where the shot noise is negligible. Recall that $\mathbf{x}_{N_s}^{(i)} = \left(\frac{1}{N_s} \sum_{j=1}^{N_s} x_{1,j}^{(i)}, \dots, \frac{1}{N_s} \sum_{j=1}^{N_s} x_{N_s,j}^{(i)} \right)^\top$, which represents

the feature vector of the i -th training circuit, and $y^{(i)}$ is the corresponding label. Solving the Lasso regression in Eq. (7) defined on the training set of size T , we obtain a solution

$$\mathbf{c}_T^{N_s} \in \operatorname{argmin}_{\|\mathbf{c}\|_1 \leq \gamma} \mathbf{c}^\top \mathbf{A}_T^{N_s} \mathbf{c} - 2 \left(\mathbf{b}_T^{N_s} \right)^\top \mathbf{c} + Y_T,$$

where we define $\mathbf{A}_T^{N_s} := \frac{1}{T} \sum_{i=1}^T \mathbf{x}_{N_s}^{(i)} \mathbf{x}_{N_s}^{(i)\top}$, $\mathbf{b}_T^{N_s} := \frac{1}{T} \sum_{i=1}^T \left(\left(\frac{1}{N_s} \sum_j x_{1,j}^{(i)} \right) y^{(i)}, \dots, \left(\frac{1}{N_s} \sum_j x_{N,j}^{(i)} \right) y^{(i)} \right)^\top$, and $Y_T := \frac{1}{T} \sum_{i=1}^T (y^{(i)})^2$. Since the solution to the Lasso regression may not be unique, we assume $\mathbf{c}_T^{N_s}$ is one of the solutions returned by the optimization algorithm.

According to the proof for Corollary 1, the MSE of using $\mathbf{c}_T^{N_s}$ to predict the labels on the test set is given by

$$L(\mathbf{c}_T^{N_s}) := \mathbf{c}_T^{N_s\top} \mathbf{A}_T^{N_s} \mathbf{c}_T^{N_s} - 2\mathbf{b}^\top \mathbf{c}_T^{N_s} + Y,$$

where we have defined $\mathbf{A}^{N_s} := \mathbb{E}_{P_{\text{test}}} [\mathbf{A} + \mathbf{A}_{N_s}]$, $\mathbf{b} := \mathbb{E}_{P_{\text{test}}} (x_1 y, \dots, x_N y)^\top$, and $Y := \mathbb{E}_{P_{\text{test}}} [y^2]$. Now, consider an arbitrary solution obtained from Eq. (7) defined on the test set, i.e.,

$$\mathbf{c}_*^{N_s} \in \operatorname{argmin}_{\|\mathbf{c}\|_1 \leq \gamma} \mathbf{c}^\top \mathbf{A}^{N_s} \mathbf{c} - 2\mathbf{b}^\top \mathbf{c} + Y.$$

Then, the MSE of applying $\mathbf{c}_*^{N_s}$ to perform QEM on the test dataset reads

$$L(\mathbf{c}_*^{N_s}) := \mathbf{c}_*^{N_s\top} \mathbf{A}^{N_s} \mathbf{c}_*^{N_s} - 2\mathbf{b}^\top \mathbf{c}_*^{N_s} + Y.$$

Note that $L(\mathbf{c}_*^{N_s})$ is the infimum of the MSE that can be achieved on the test dataset with Lasso regression when $T \rightarrow \infty$.

Next, we estimate the size of the training set T required such that

$$L(\mathbf{c}_T^{N_s}) \leq L(\mathbf{c}_*^{N_s}) + \varepsilon$$

with probability at least $1 - \delta$. We first present the following lemma, which characterizes the relationship between the MSE on the training set and that on the test set using the same coefficients \mathbf{c} .

Lemma 3. *For arbitrary $\|\mathbf{c}\|_1 \leq \gamma$, a training set of size $T \geq \ln \left(\frac{6N^2}{\delta} \right) \frac{(12\gamma^2\|\mathcal{O}\|^2)^2}{\varepsilon^2} \in \mathcal{O} \left(\ln \left(\frac{N}{\delta} \right) \frac{1}{\varepsilon^2} \right)$ suffices to obtain $\mathbf{A}_T^{N_s}, \mathbf{b}_T^{N_s}$ and Y_T such that*

$$L(\mathbf{c}) - \varepsilon/2 \leq \mathbf{c}^\top \mathbf{A}_T^{N_s} \mathbf{c} - 2 \left(\mathbf{b}_T^{N_s} \right)^\top \mathbf{c} + Y_T \leq L(\mathbf{c}) + \varepsilon/2$$

with probability at least $1 - \delta$.

A similar result to the above lemma can be found in [54, Chapter 11]. To make this paper self-contained, we provide a proof here.

Proof. We begin by deriving an upper bound for the difference in MSE between the training set of size T and the test set, using the same coefficients \mathbf{c} .

$$\begin{aligned} & \left| \mathbf{c}^\top \mathbf{A}_T^{N_s} \mathbf{c} - 2 \left(\mathbf{b}_T^{N_s} \right)^\top \mathbf{c} + Y_T - (\mathbf{c}^\top \mathbf{A}^{N_s} \mathbf{c} - 2\mathbf{b}^\top \mathbf{c} + Y) \right| \\ & \leq \left| \mathbf{c}^\top \mathbf{A}_T^{N_s} \mathbf{c} - \mathbf{c}^\top \mathbf{A}^{N_s} \mathbf{c} \right| + 2 \left| \left(\mathbf{b}_T^{N_s} \right)^\top \mathbf{c} - \mathbf{b}^\top \mathbf{c} \right| + |Y_T - Y| \\ & \leq \|\mathbf{c}\|_1 \left\| (\mathbf{A}_T^{N_s} - \mathbf{A}^{N_s}) \mathbf{c} \right\|_\infty + 2\|\mathbf{c}\|_1 \left\| \mathbf{b}_T^{N_s} - \mathbf{b} \right\|_\infty + |Y_T - Y| \\ & \leq \gamma^2 \left\| \mathbf{A}_T^{N_s} - \mathbf{A}^{N_s} \right\|_{\max} + 2\gamma \left\| \mathbf{b}_T^{N_s} - \mathbf{b} \right\|_\infty + |Y_T - Y|, \end{aligned}$$

where the max (infinity) norm of a matrix (vector) is the maximum absolute value of its entries. As in Lemma 1 and Theorem 7, each entry of $\mathbf{A}^{N_s}, \mathbf{b}$ and Y is the expectation value of a certain

random variable, and each corresponding entry of $\mathbf{A}_T^{N_s}, \mathbf{b}_T^{N_s}$ and Y_T is an approximation of the expectation value using T samples. Meanwhile, the absolute values of these random variables are upper bounded:

$$\begin{aligned} \left| \frac{1}{N_s} \sum_{l=1}^{N_s} x_{j,l}^{(i)} \frac{1}{N_s} \sum_{l=1}^{N_s} x_{k,l}^{(i)} \right| &\leq \|O\|^2, \\ \left| \frac{1}{N_s} \sum_{l=1}^{N_s} x_{j,l}^{(i)} y^{(i)} \right| &\leq \|O\|^2, \left(y^{(i)} \right)^2 \leq \|O\|^2, \end{aligned}$$

for arbitrary $j, k \in [N]$ and $i \in [T]$, where $\|O\|$ denotes the spectral norm of the observable O . As a result, by Hoeffding's inequality we have that

$$\begin{aligned} \Pr \left(\left| \frac{1}{T} \sum_{i=1}^T \left(\frac{1}{N_s} \sum_{l=1}^{N_s} x_{j,l}^{(i)} \right) \left(\frac{1}{N_s} \sum_{l=1}^{N_s} x_{k,l}^{(i)} \right) - (\mathbf{A}^{N_s})_{j,k} \right| \geq \frac{\varepsilon}{6\gamma^2} \right) &\leq \frac{\delta}{3N^2}, \\ \Pr \left(\left| \frac{1}{T} \sum_{i=1}^T \left(\frac{1}{N_s} \sum_{l=1}^{N_s} x_{j,l}^{(i)} \right) y^{(i)} - (\mathbf{b})_j \right| \geq \frac{\varepsilon}{12\gamma} \right) &\leq \frac{\delta}{3N}, \\ \Pr \left(\left| \frac{1}{T} \sum_{i=1}^T \left(y^{(i)} \right)^2 - \mathbb{E}_{P_{\text{test}}} y^2 \right| \geq \frac{\varepsilon}{6} \right) &\leq \frac{\delta}{3}, \end{aligned}$$

provided $T \geq \ln \left(\frac{6N^2}{\delta} \right) \frac{(12\gamma^2\|O\|^2)^2}{\varepsilon^2} \in \mathcal{O} \left(\ln \left(\frac{N}{\delta} \right) \frac{1}{\varepsilon^2} \right)$. By the union bound, the inequalities

$$\begin{aligned} \left\| \mathbf{A}_T^{N_s} - \mathbf{A}^{N_s} \right\|_{\max} &\leq \frac{\varepsilon}{6\gamma^2} \\ \left\| \mathbf{b}_T^{N_s} - \mathbf{b} \right\|_{\infty} &\leq \frac{\varepsilon}{12\gamma} \\ |Y_T - Y| &\leq \frac{\varepsilon}{6} \end{aligned}$$

hold at the same time with probability at least $1 - \delta$. Then we have that

$$\begin{aligned} &\left| \mathbf{c}^\top \mathbf{A}_T^{N_s} \mathbf{c} - 2 \left(\mathbf{b}_T^{N_s} \right)^\top \mathbf{c} + Y_T - (\mathbf{c}^\top \mathbf{A}^{N_s} \mathbf{c} - 2\mathbf{b}^\top \mathbf{c} + Y) \right| \\ &\leq \gamma^2 \left\| \mathbf{A}_T^{N_s} - \mathbf{A}^{N_s} \right\|_{\max} + 2\gamma \left\| \mathbf{b}_T^{N_s} - \mathbf{b} \right\|_{\infty} + |Y_T - Y| \\ &\leq \gamma^2 \frac{\varepsilon}{6\gamma^2} + 2\gamma \frac{\varepsilon}{12\gamma} + \frac{\varepsilon}{6} \\ &\leq \varepsilon/2 \end{aligned}$$

holds with probability at least $1 - \delta$, which concludes the proof. \square

Based on Lemma 3, we next prove the following theorem.

Theorem 8. *A training set*

$$\mathbb{S} = \left\{ \left(\left(x_1^{(i)}, \dots, x_N^{(i)} \right), y^{(i)} \right) \right\}_{i=1, \dots, T}$$

of size

$$T \geq \ln \left(\frac{6N^2}{\delta} \right) \frac{(12\gamma^2\|O\|^2)^2}{\varepsilon^2} \in \mathcal{O} \left(\ln \left(\frac{N}{\delta} \right) \frac{1}{\varepsilon^2} \right)$$

suffices to obtain a solution $\mathbf{c}_T^{N_s}$ such that

$$L(\mathbf{c}_T^{N_s}) \leq L(\mathbf{c}_*^{N_s}) + \varepsilon$$

with probability at least $1 - \delta$.

Proof. According to Lemma 3, given $T \geq \ln\left(\frac{6N^2}{\delta}\right) \frac{(12\gamma^2\|O\|^2)^2}{\varepsilon^2} \in \mathcal{O}\left(\ln\left(\frac{N}{\delta}\right) \frac{1}{\varepsilon^2}\right)$, we have that

$$\begin{aligned} & \mathbf{c}_T^{N_s \top} \mathbf{A}_T^{N_s} \mathbf{c}_T^{N_s} - 2 \left(\mathbf{b}_T^{N_s} \right)^\top \mathbf{c}_T^{N_s} + Y_T \\ &= \min_{\|\mathbf{c}\|_1 \leq \gamma} \mathbf{c}^\top \mathbf{A}_T^{N_s} \mathbf{c} - 2 \left(\mathbf{b}_T^{N_s} \right)^\top \mathbf{c} + Y_T \\ &\leq \mathbf{c}_*^{N_s \top} \mathbf{A}_T^{N_s} \mathbf{c}_*^{N_s \top} - 2 \left(\mathbf{b}_T^{N_s} \right)^\top \mathbf{c}_*^{N_s \top} + Y_T \\ &\leq \mathbf{c}_*^{N_s \top} \mathbf{A}^{N_s} \mathbf{c}_*^{N_s} - 2 \mathbf{b}^\top \mathbf{c}_*^{N_s} + Y + \varepsilon/2 \end{aligned}$$

with probability at least $1 - \delta$. Then we have that

$$\begin{aligned} & L(\mathbf{c}_T^{N_s}) - L(\mathbf{c}_*^{N_s}) \\ &= \mathbf{c}_T^{N_s \top} \mathbf{A}^{N_s} \mathbf{c}_T^{N_s} - 2 \mathbf{b}^\top \mathbf{c}_T^{N_s} + Y - (\mathbf{c}_*^{N_s \top} \mathbf{A}^{N_s} \mathbf{c}_*^{N_s} - 2 \mathbf{b}^\top \mathbf{c}_*^{N_s} + Y) \\ &\leq \mathbf{c}_T^{N_s \top} \mathbf{A}^{N_s} \mathbf{c}_T^{N_s} - 2 \mathbf{b}^\top \mathbf{c}_T^{N_s} + Y - \left(\mathbf{c}_T^{N_s \top} \mathbf{A}_T^{N_s} \mathbf{c}_T^{N_s} - 2 \left(\mathbf{b}_T^{N_s} \right)^\top \mathbf{c}_T^{N_s} + Y_T \right) + \varepsilon/2. \end{aligned}$$

Since $\|\mathbf{c}_T^{N_s}\|_1 \leq \gamma$, according to Lemma 3, it holds that

$$\mathbf{c}_T^{N_s \top} \mathbf{A}^{N_s} \mathbf{c}_T^{N_s} - 2 \mathbf{b}^\top \mathbf{c}_T^{N_s} + Y - \left(\mathbf{c}_T^{N_s \top} \mathbf{A}_T^{N_s} \mathbf{c}_T^{N_s} - 2 \left(\mathbf{b}_T^{N_s} \right)^\top \mathbf{c}_T^{N_s} + Y_T \right) \leq \varepsilon/2,$$

which implies that $L(\mathbf{c}_T^{N_s}) - L(\mathbf{c}_*^{N_s}) \leq \varepsilon$. \square

C.2 Time Complexity of NIL

We analyze the time complexity of our method. Suppose the number of neighbor circuits is N , and we want the test MSE of our model to be smaller than ε with probability at least $1 - \delta$. We estimate the cost of our approach. We first estimate the number of shots N_s needed to measure the involved circuits. Note that the MSE derived from the optimal coefficients $\mathbf{c}_*^{N_s}$ is given by

$$\mathbf{c}_*^{N_s \top} \mathbb{E}_{P_{\text{test}}} [A + \mathbf{\Lambda}_{N_s}] \mathbf{c}_*^{N_s} - 2 \mathbf{b}^\top \mathbf{c}_*^{N_s} + \mathbb{E}_{P_{\text{test}}} [y^2].$$

Since $X_i \leq \|O^2\|$ and $\|\mathbf{c}_*^{N_s}\|_1 \leq \gamma$, the regularization term introduced by shot noise is upper bounded by

$$\begin{aligned} \mathbf{c}_*^{N_s \top} \mathbb{E}_{P_{\text{test}}} [\mathbf{\Lambda}_{N_s}] \mathbf{c}_*^{N_s} &= \mathbf{c}_*^{N_s \top} \mathbb{E}_{P_{\text{test}}} \left[\frac{\text{diag}(X_1, \dots, X_N)}{N_s} \right] \mathbf{c}_*^{N_s} \\ &\leq \|O^2\| \gamma^2 / N_s. \end{aligned}$$

To ensure that this term does not dominate the error in the MSE, we impose the condition $\|O^2\| \gamma^2 / N_s \leq \varepsilon$, which gives that $N_s \geq \|O^2\| \gamma^2 / \varepsilon$. It is worth noting that the above expression may be rather conservative and far from the tight condition on the number of shots required to achieve an MSE of ε . In the numerical experiments, we observe that using N_s shots to estimate the expectation value can yield an MSE that is significantly smaller than $\|O^2\| \gamma^2 / N_s$.

In the following, we treat N_s as a constant satisfying the above condition. The time complexity of our approach can be estimated through the following steps: generating the training set, computing the optimal coefficients given in Eq. (7), and applying the learned coefficients to mitigate noise in the target circuit. Below, we discuss the time complexity of each step individually.

Generating the training set. To generate a training set of the form

$$\mathbb{S}^{N_s} = \left\{ \left(\left(\frac{1}{N_s} \sum_{j=1}^{N_s} x_{1,j}^{(i)}, \dots, \frac{1}{N_s} \sum_{j=1}^{N_s} x_{N,j}^{(i)} \right), y^{(i)} \right) \right\}_{i \in [T]},$$

we need to compute the feature vector $\left(\frac{1}{N_s} \sum_{j=1}^{N_s} x_{1,j}^{(i)}, \dots, \frac{1}{N_s} \sum_{j=1}^{N_s} x_{N,j}^{(i)}\right)$ and the label $y^{(i)}$ for each training circuit generated by 2-training method. The number of training circuits we generate is $T = \mathcal{O}\left(\ln\left(\frac{N}{\delta}\right) \frac{1}{\varepsilon^2}\right)$. This choice can be justified as follows. As proved in Subsection C.1, a training set of size $T = \mathcal{O}\left(\ln\left(\frac{N}{\delta}\right) \frac{1}{\varepsilon^2}\right)$ suffices to obtain a solution $\mathbf{c}_t^{N_s}$ whose test MSE is smaller than the optimal test MSE plus ε . If the optimal test MSE is already smaller than ε , then the test MSE of $\mathbf{c}_t^{N_s}$ will be below 2ε , which is acceptable. However, if the test MSE of $\mathbf{c}_t^{N_s}$ exceeds 2ε , the optimal MSE must be larger than ε . In this case, we should increase the number of neighbor circuits rather than the number of training circuits.

After generating the training circuits, we apply the neighbor map to these circuits and measure $\mathcal{O}(TN) = \mathcal{O}\left(\ln\left(\frac{N}{\delta}\right) \frac{N}{\varepsilon^2}\right)$ neighbor circuits (with N neighbor circuits for each training circuit) for N_s times. The expectation values for the ideal training circuits can be simulated efficiently, as they are all Clifford circuits. The labels $y^{(i)}$'s can be efficiently computed classically in $\mathcal{O}(T \text{poly}(n))$ time, where n is the number of qubits.

In our numerical experiments, we observe that the training set size required for convergence is significantly smaller than the theoretical bound. Specifically, empirical data fitting suggests that the training MSE converges when the training set size follows the approximate scaling

$$T = \frac{2\gamma \ln N}{\sqrt{\varepsilon}},$$

where γ is some constant. Based on this empirical scaling, it appears sufficient in practice to generate approximately $\mathcal{O}(TN) = \mathcal{O}\left(\frac{N \ln N}{\sqrt{\varepsilon}}\right)$ neighbor circuits.

Computing the optimal coefficients. This step can be completed on classical computers. Many algorithms have been developed to solve the optimization problem Eq. (7) [55, 56, 57, 58]. Particularly, we can solve this problem with the algorithm in [55] in time $\mathcal{O}(N^3 + TN^2) = \mathcal{O}(N^3)$.

The above two steps constitute the entire training stage, where we generate $\mathcal{O}(TN) = \mathcal{O}\left(\ln\left(\frac{N}{\delta}\right) \frac{N}{\varepsilon^2}\right)$ quantum circuits, and the running time on a classical computer is upper bounded by

$$\mathcal{O}(T(\text{poly}(n)) + N^3) = \mathcal{O}\left(\ln\left(\frac{N}{\delta}\right) \frac{\text{poly}(n)}{\varepsilon^2} + N^3\right).$$

The coefficients returned by the classical computer for QEM are applicable to all target circuits with the same structure, i.e., circuits that differ only in the parameters of the rotation gates. Next, we utilize the learned coefficients to perform QEM on the target circuit.

Applying the learned model. After obtaining the coefficients $\mathbf{c}_t^{N_s}$, for a target circuit requiring QEM, we only need to measure its N neighbor circuits N_s times to collect the feature vector \mathbf{x}_{N_s} . Finally, we output the mitigated target expectation value as $\mathbf{c}_t^{N_s \top} \mathbf{x}_{N_s}$, which can be computed in $\mathcal{O}(N)$ time.

As we can see, once the coefficients are learned, applying our method to the target circuit is very efficient, requiring significantly less time compared to the training phase. We emphasize that the computational resources consumed in the training stage are worthwhile, as the learned coefficients can be applied to all parameter configurations of the target circuit.

D Benchmarking Performance on Large-scale Non-Clifford Circuits

In this section, we demonstrate that the performance of NIL can be reliably benchmarked even on large non-Clifford circuits, a regime that poses significant challenges for previous learning-based QEM protocols. Owing to the specific mathematical structure of the 2-design training method, we can establish the following corollary:

Corollary 2. *For an arbitrary $\mathbf{c} = (c_1, c_2, \dots, c_N)^\top$,*

$$\mathbb{E}_{\text{train}} \left(\mathbf{c}^\top \cdot \mathbf{x}_{N_s} - y \right)^2 = \mathbb{E}_{\text{test}} \left(\mathbf{c}^\top \cdot \mathbf{x}_{N_s} - y \right)^2.$$

Proof. We directly substitute \mathbf{c} to the target circuit. According to Theorem 7, we have

$$\begin{aligned}
& \mathbb{E}_{\text{test}} (\mathbf{c}^\top \cdot \mathbf{x}_{N_s} - y)^2 \\
&= \mathbb{E}_{\text{test}} (\mathbf{c}^\top \cdot \mathbf{x}_{N_s} - y) (\mathbf{c}^\top \cdot \mathbf{x}_{N_s} - y)^\top \\
&= \mathbf{c}^\top \mathbb{E}_{\text{test}} [\mathbf{x}_{N_s} \mathbf{x}_{N_s}^\top] \mathbf{c} - 2\mathbf{c}^\top \mathbb{E}_{\text{test}} [y \mathbf{x}_{N_s}] + \mathbb{E}_{\text{test}} y^2 \\
&= \mathbf{c}^\top \mathbb{E}_{\text{train}} [\mathbf{x}_{N_s} \mathbf{x}_{N_s}^\top] \mathbf{c} - 2\mathbf{c}^\top \mathbb{E}_{\text{train}} [y \mathbf{x}_{N_s}] + \mathbb{E}_{\text{test}} y^2 \\
&= \mathbb{E}_{\text{train}} (\mathbf{c}^\top \cdot \mathbf{x}_{N_s} - y)^2.
\end{aligned}$$

□

Corollary 2 reveals an important fact: when a learning-based QEM protocol employs linear regressions to fit the training data, the set of training circuits generated by 2-training method can also efficiently benchmark the obtained model's actual performance on the target parameterized circuit in the average sense, provided the neighbor circuits of both training and target circuits are measured with the same number of shots.

To understand this, note that the MSE achieved on the training circuits generated by 2-training method can be computed classically and efficiently, whereas the MSE for target parameterized circuits is difficult to obtain even with quantum computers, since ideal expectation values cannot be efficiently simulated classically. Therefore, Corollary 2 enables us to estimate our protocol's performance on large non-Clifford quantum circuits on average without requiring precise classical simulation of the ideal target expectation values.

E Mean Squared Error and Worst Case Error

We have shown that the learning-based QEM model using our approach to generate training circuits yields the optimal linear function (with respect to MSE) on average. In this section, we prove that if the MSE on the training dataset is low, then for any specific parameter configuration of the target quantum circuit, there is a high probability of obtaining good error mitigation performance.

Let the MSE achieved on the training circuit be ε , i.e.,

$$\mathbb{E}_{\text{train}} (\mathbf{c}^\top \cdot \mathbf{x}_{N_s} - y)^2 = \varepsilon.$$

According to Corollary 2, we have

$$\mathbb{E}_{\text{test}} (\mathbf{c}^\top \cdot \mathbf{x}_{N_s} - y)^2 = \mathbb{E}_{\text{train}} (\mathbf{c}^\top \cdot \mathbf{x}_{N_s} - y)^2 = \varepsilon.$$

By Jensen's inequality, we derive that

$$\left(\mathbb{E}_{\text{test}} |\mathbf{c}^\top \cdot \mathbf{x}_{N_s} - y| \right)^2 \leq \mathbb{E}_{\text{test}} (\mathbf{c}^\top \cdot \mathbf{x}_{N_s} - y)^2 = \varepsilon,$$

which yields

$$\mathbb{E}_{\text{test}} |\mathbf{c}^\top \cdot \mathbf{x}_{N_s} - y| \leq \sqrt{\varepsilon}.$$

Therefore, for any instance of (\mathbf{x}'_{N_s}, y') , which is obtained by measuring each neighbor circuit of the target circuit for N_s times, by Chebyshev's inequality it holds that

$$\Pr \left(\left| |\mathbf{c}^\top \cdot \mathbf{x}'_{N_s} - y'| - \mathbb{E}_{\text{test}} |\mathbf{c}^\top \cdot \mathbf{x}_{N_s} - y| \right| \geq k\sqrt{\varepsilon} \right) \leq \frac{\text{Var} |\mathbf{c}^\top \cdot \mathbf{x}_{N_s} - y|}{k^2 \varepsilon} \leq \frac{1}{k^2}.$$

This suggests that on any specific parameter configuration of the target quantum circuit, the protocol can achieve

$$|\mathbf{c}^\top \cdot \mathbf{x}'_{N_s} - y'| \leq k\sqrt{\varepsilon} + \sqrt{\varepsilon} = (k+1)\sqrt{\varepsilon}$$

with probability at least $1 - \frac{1}{k^2}$.

For instance, if the MSE on the training set is less than 10^{-4} (which is easily achievable for all the quantum circuits we have numerically studied) and we choose $k = 10$, then our approach ensures that on any specific parameter configuration of the target circuit, the error in the output expectation value will be less than 0.1 with probability exceeding 99%. Note that we do not rule out the possibility of encountering certain parameter configurations with larger errors. However, the above discussion implies that their occurrence is statistically improbable. In fact, we have conducted various numerical experiments on different quantum circuits to investigate the QEM performance for individual circuits. In all cases we have studied (as detailed in Subsection E.1), when a good QEM protocol is discovered in terms of MSE, the expectation values are recovered to be very close to the ideal values for all test circuits.

E.1 Low Mean Squared Error May Indicate Low Worst-Case Error

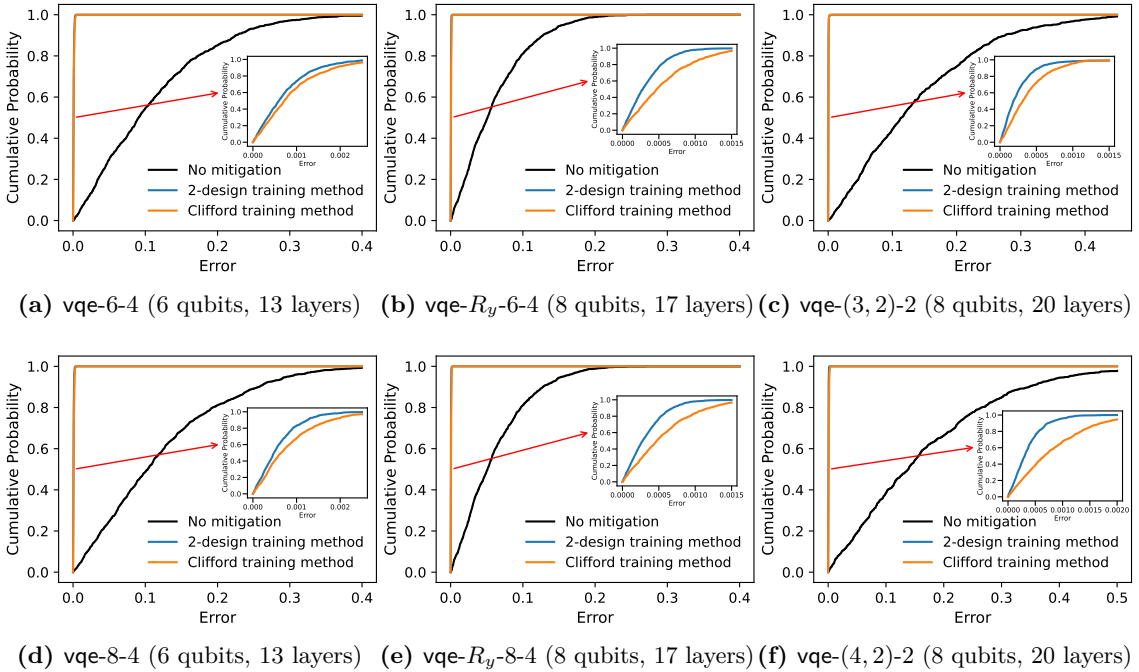


Figure 8: Empirical cumulative distribution of the computing error for 500 random parameter configurations of the target quantum circuit. For each point (x, y) on the curve, x represents the absolute deviation from the ideal expectation value, and y denotes the proportion of configurations (out of 500) with an absolute deviation less than x . In the main figures, the blue and orange curves nearly coincide. The insets zoom in on the region where the curves diverge, specifically when the error approaches zero. The results show that the blue curve (obtained using the 2-design method) yields a more accurate prediction of the ideal expectation value with higher probability compared to the orange curve (obtained using the Clifford training method).

We perform numerical simulations for a specific error mitigation task to evaluate the performance of our protocol on individual parameter configurations of the target quantum circuit. Recall that our protocol guarantees the optimal linear solution in the average case.

Here all the weight-1 Pauli neighbors are chosen to serve as neighbor circuits, as depicted in Fig. 8. We find that for all the parameter configurations where we could classically calculate the ideal expectation values, the worst-case error of our protocol is less than 3×10^{-3} . This indicates that our method not only has excellent error mitigation effects on average, but also has a low failure probability.

We also compare the performance of our method with the Clifford training method, which uses all Clifford gates. As shown in the insets of Fig. 8, our method achieves lower error with higher probability across all cases.

F Using Non-Clifford Quantum Circuits for Training

In this section, we show that retaining a subset of non-Clifford gates when generating the training circuits helps the model learn more efficiently. We first show a limitation of Clifford training circuits in learning the pattern of quantum noise. When considering only Pauli noise channels and a Pauli observable O , if a neighbor circuit $C_j^{(i)}$ is obtained by inserting Pauli gates to a Clifford training circuit $C^{(i)}$, then it can be proven that $\langle \tilde{C}_j^{(i)} \rangle = \pm \langle \tilde{C}^{(i)} \rangle$, where $\langle \tilde{C} \rangle$ is the noisy target expectation value obtained on C .

Lemma 4. *Suppose a Clifford quantum circuit C_j can be expressed as $C_j = U_m \cdots U_1$, and a noisy implementation of C_j is given by*

$$\tilde{C}_j = \mathcal{E}_m \circ \mathcal{P}_m \circ \mathcal{U}_m \cdots \mathcal{E}_1 \circ \mathcal{P}_1 \circ \mathcal{U}_1,$$

where \mathcal{E}_j is a Pauli noise channel, \mathcal{U}_j is a Clifford gate, and \mathcal{P}_j is a Pauli gate or the product of two Pauli gates. Then $\langle \tilde{C}_j^{(i)} \rangle = \pm \langle \tilde{C}^{(i)} \rangle$.

Proof. Since \mathcal{E}_m is a Pauli noise channel, we have that $\mathcal{E}_m \circ \mathcal{P}_m = \mathcal{P}_m \circ \mathcal{E}_m$. In this way, \mathcal{P}_m can be moved to the end of the circuit. Similarly, \mathcal{P}_{m-1} commutes with \mathcal{E}_{m-1} . As U_m is a Clifford gate; that is, $U_m P_{m-1} \rho P_{m-1} U_m^\dagger = P'_{m-1} U_m \rho U_m^\dagger P'_{m-1}$, where P'_{m-1} is also a Pauli operator. Then the quantum channel \mathcal{P}'_{m-1} commutes with \mathcal{E}_m and can also be moved to the end of the circuit, which combined with \mathcal{P}_m becomes another Pauli operator.

Repeating this process, we move all the inserted Pauli gates to the end of the circuit, resulting in

$$\tilde{C}_j = \mathcal{Q} \circ \mathcal{E}_m \circ \mathcal{U}_m \cdots \mathcal{E}_1 \circ \mathcal{U}_1,$$

where \mathcal{Q} is a Pauli channel. Therefore, we have that

$$\begin{aligned} \langle \tilde{C}_j \rangle &= \text{tr}(O \tilde{C}_j(\rho_{\text{in}})) \\ &= \text{tr}(O \mathcal{Q} \circ \mathcal{E}_m \circ \mathcal{U}_m \cdots \mathcal{E}_1 \circ \mathcal{U}_1(\rho_{\text{in}})) \\ &= \text{tr}((Q^\dagger O Q) \mathcal{E}_m \circ \mathcal{U}_m \cdots \mathcal{E}_1 \circ \mathcal{U}_1(\rho_{\text{in}})) \\ &= \mu(Q, O) \text{tr}(O \tilde{C}(\rho_{\text{in}})) \\ &= \mu(Q, O) \langle \tilde{C} \rangle, \end{aligned}$$

where $\mu(Q, O)$ is 1 if Q and O commute and -1 otherwise. \square

Algorithm 3 Strategy for constructing training circuits including non-Clifford ones

Input: Target parameterized circuit $C(\theta)$ and the depth L for the non-Clifford layer

Output: A set \mathbb{S} of training circuits

```

1:  $S \leftarrow \emptyset$ 
2: for  $i = 1, 2, \dots, T$  do
3:   for each gate in the circuit  $C(\theta)$  do
4:     if the gate is of the form  $R_\sigma(\theta)$  ( $\sigma = x, y, z$ ) then
5:       if the current layer  $l > L$ , then
6:          $\theta \leftarrow \mathbb{S} \{0, \pi/2, \pi, 3\pi/2\}$ 
7:       else
8:          $\theta \leftarrow \mathbb{S} [0, 2\pi)$ 
9:       end if
10:      end if
11:    end for
12:    Add the new circuit to  $\mathbb{S}$ 
13: end for

```

Lemma 4 implies that the noisy expectation value of each training circuit $C^{(i)}$ and those of all its neighbor circuits $C_j^{(i)}$ are either the same or the opposite in this case. Consequently, all data

points in the training set are of the form $((x^{(i)}, \pm x^{(i)}, \pm x^{(i)}, \dots), y^{(i)})$ with $x^{(i)} = \langle \widetilde{\mathcal{C}^{(i)}} \rangle$ and the noiseless expectation value $y^{(i)} \in \{0, \pm 1\}$ [59]. This creates a significant discrepancy between the training set and the test set generated from the target quantum circuits, which could seriously hinder the learning process.

A possible way to address this issue is to introduce training circuits of the form $C^{(i)} = U^{(i)}V^{(i)}$, where $U^{(i)}$ is a Clifford circuit and $V^{(i)}$ is a shallow quantum circuit that may contain non-Clifford gates. To achieve this, we can modify 2-training method by setting the angles of the rotation gates in the first few layers of $C^{(i)}$ to be uniformly distributed in $[0, 2\pi)$, which forms $V^{(i)}$, as illustrated in Fig. 9. The pseudo-code for this strategy is presented in Algorithm 3.

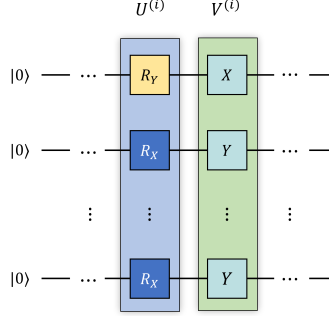


Figure 9: Non-Clifford training circuits. It is produced by first applying 2-training method on the target circuit, and then replacing the first layer by non-Clifford gates.

When the observable O is a Pauli operator or a sum of polynomially many Pauli operators, the expectation value $\langle \mathcal{C}^{(i)} \rangle$ can be classically computed. Indeed, suppose for simplicity that O is a Pauli operator, then the ideal expectation value is given by

$$\langle \mathcal{C}^{(i)} \rangle = \text{tr}(O U^{(i)} \circ \mathcal{V}^{(i)}(\rho_{\text{in}})) = \text{tr}(O' \mathcal{V}^{(i)}(\rho_{\text{in}})),$$

where $O' := (U^{(i)})^\dagger O U^{(i)}$ is also a Pauli operator by the definition of Clifford circuits. In such a situation, computing the expectation value for $C^{(i)}$ is reduced to computing that for $V^{(i)}$, which can then be classically computed by tensor network methods [60]. For the computation of $\langle \mathcal{C}^{(i)} \rangle$ to be efficient, we require the depth of $V^{(i)}$ to be $O(\log n)$, where n is the number of input qubits.

F.1 Comparison Between Mixed and Purely Clifford Training Circuits

Next we compare the performance of a learning-based QME protocol employing shallow non-Clifford circuits for training with that of a protocol employing only Clifford training circuits. Specifically, in the first one or two layers of each training circuit, we allow non-Clifford gates (i.e., rotation gates with random angles), while the remaining layers are still generated by 2-training method. Here, we choose all the weight-1 neighbors as the neighbor circuits, and the learning model remains a linear function. It can be seen that both protocols successfully converge to the optimal linear function. We then compare the convergence speeds of these two protocols to the solutions, particularly the sizes of the training circuit sets required to achieve stable convergence.

As shown in Fig. 10, the protocol using non-Clifford training circuits exhibits a smoother convergence curve, indicating a faster convergence rate. Therefore, in practical applications, we can reduce the number of training circuits required by introducing shallow non-Clifford gate layers into the training circuits.

G Producing Training Circuits with All the Single-Qubit Clifford Gates

In this section, we show that the Clifford training method performs well only when the single-qubit gates in the target circuits are drawn from the Haar random distribution. This discrepancy arises

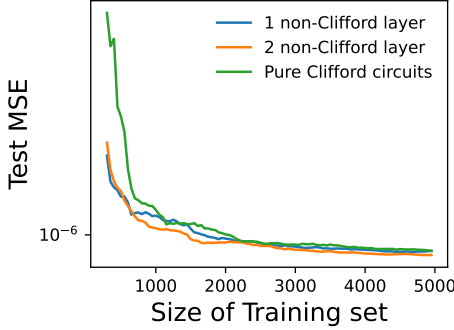


Figure 10: Comparison between the performance of learning-based QEM models with purely Clifford training circuits and that with non-Clifford training circuits. The underlying circuit is vqe-6-4.

because Clifford gates do not form a quantum rotation 2-design, but rather a unitary 2-design with respect to Haar random unitaries. Suppose the training set

$$\mathbb{S}' = \left\{ \left(\left(x_1^{(i)}, \dots, x_N^{(i)} \right), y^{(i)} \right) \right\}_{i=1, \dots, |\mathbb{S}'|}$$

is generated by Clifford training method, i.e., all the single-qubit Clifford gates are utilized to replace each non-Clifford single-qubit gates in target circuits. Let $P_{\mathbb{S}'}^*$ be the probability distribution of the data in \mathbb{S}' , when the parameters of the target quantum circuit are uniformly distributed within $[0, 2\pi]$. As in Subsection B.2, we can derive that the solution to the linear regression that fits the data in \mathbb{S}' is expressed as

$$\left(\mathbb{E}_{P_{\mathbb{S}'}^*} [\mathbf{A}] \right)^{-1} \mathbb{E}_{P_{\mathbb{S}'}^*} [\mathbf{a}], \quad (18)$$

where we write $\mathbb{E}_{(\mathbf{x}, y) \sim P_{\mathbb{S}'}}$ as $\mathbb{E}_{P_{\mathbb{S}'}}$ for simplicity and the definitions of \mathbf{A} and \mathbf{a} can be found in Eq. (10).

If $\mathbb{E}_{P_{\mathbb{S}'}} [\mathbf{x} \cdot \mathbf{x}^\top]$ is not invertible, then we can use the pseudoinverse. Repeating the proof in Lemma 1, and using the fact that the Clifford group forms a unitary 3-design [61], we have

$$\begin{aligned} & \mathbb{E}_{g \in C_1} \text{tr} \left(g \otimes I \rho g^\dagger \otimes I \Phi_2^\dagger(O) \right) \text{tr} \left(g \otimes I \rho' g^\dagger \otimes I \Phi_2'^\dagger(O) \right) \\ &= \mathbb{E}_{U_1 \sim \text{haar}} \text{tr} \left(U_1 \otimes I \rho U_1^\dagger \otimes I \Phi_2^\dagger(O) \right) \text{tr} \left(U_1 \otimes I \rho' U_1^\dagger \otimes I \Phi_2'^\dagger(O) \right). \end{aligned}$$

By a similar proof as in Lemma 1, we can directly derive the following conclusion.

Lemma 5. *Consider a new set of test circuits, where the circuits have a same structure with the original test circuit, with the difference being that the non-Clifford gates are not fixed-axis rotation gates, but Haar random single-qubit gates. Then we have*

$$\mathbb{E}_{P_{\mathbb{S}'}} [\mathbf{A}] = \mathbb{E}_{P_{\text{test}'}} [\mathbf{A}] \text{ and } \mathbb{E}_{P_{\mathbb{S}'}} [\mathbf{a}] = \mathbb{E}_{P_{\text{test}'}} [\mathbf{a}],$$

where $P_{\text{test}'}$ is the probability distribution of the data produced by the new test set.

Based on Lemma 5, the solution in Eq. (18) equals

$$\left(\mathbb{E}_{P_{\text{test}'}} [\mathbf{A}] \right)^{-1} \mathbb{E}_{P_{\text{test}'}} [\mathbf{a}], \quad (19)$$

which indicates that in a learning-based QEM protocol, if training circuits are generated by replacing each single-qubit non-Clifford gate with all possible single-qubit Clifford gates uniformly—the conventional strategy in literature—the model will obtain the optimal linear solution on average, provided all single-qubit non-Clifford gates in the target circuit are Haar-random unitaries. This also explains the significant differences observed between protocols using different training circuit sets in the manuscript.

H Comparisons Between Different Design Choices of NIL-based QEM

We now compare different design and hyperparameter choices of NIL in a comprehensive manner.

H.1 Comparison Between Choices of Neighbor Maps

We first compare the performance of learning-based QEM models constructed with different types of neighbor circuits. The test circuit is chosen to be `vqe-6-4`, as introduced in the manuscript. Training circuits are generated using the 2-design method. For comparison, we consider three neighbor-generation strategies: Pauli-insertion neighbors, CPTP-insertion neighbors, and ZNE neighbors. The definitions of Pauli-insertion and ZNE neighbors follow those in the manuscript.

The CPTP-insertion neighbors are obtained by expanding the Pauli gate set used in Pauli-insertion neighbors to

$$\mathbb{G}_1 := \{\mathcal{X}, \mathcal{Y}, \mathcal{Z}, \mathcal{K}^\dagger \mathcal{S}^\dagger \mathcal{K}, \mathcal{K} \mathcal{S}^\dagger \mathcal{K}^\dagger, \mathcal{S}^\dagger, \mathcal{K} \mathcal{H} \mathcal{K}^\dagger, \mathcal{H}, \mathcal{K}^\dagger \mathcal{H} \mathcal{K}\},$$

where \mathcal{S} , \mathcal{H} , and \mathcal{K} are the quantum channels for the S gate, the H gate, and the $K := SH$ gate, respectively. \mathbb{G}_1 is actually a basis for the single-qubit CPTP maps when appended with the identity channel and three extra state-preparation channels [20]. Note that all the gates from \mathbb{G}_1 are single-qubit Clifford gates. For brevity, we hereafter refer to Pauli-insertion and CPTP-insertion neighbors simply as Pauli neighbors and CPTP neighbors, respectively.

The training method still adopts the Lasso regression formulation in Eq. (7), where we set $\gamma = 2$ for both Pauli neighbors and CPTP neighbors. Recall that the ZNE neighbor circuits for each training (or test) circuit are obtained by replacing each noise channel Λ with Λ^α , where $\alpha \in \{1, 1.1, 1.34, 1.58\}$. This implies that only four neighbor circuits are available for each training circuit. To improve the power of this neighbor map, we set the ℓ_1 norm restriction $\gamma = 5$ in Lasso regression for ZNE neighbors.

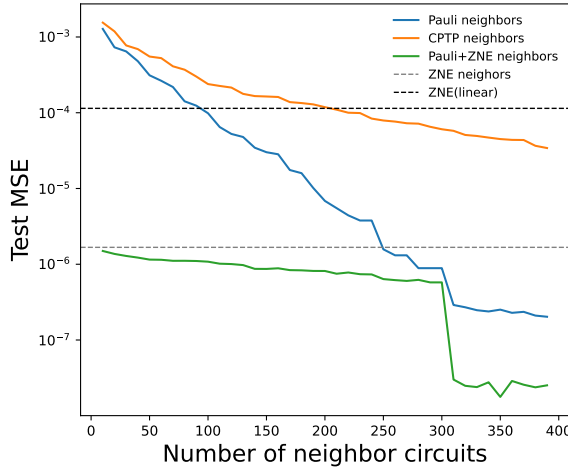


Figure 11: Performances of learning-based QEM protocols that choose different neighbor circuits. The underlying circuit is `vqe-6-4`.

The results are shown in Fig. 11. It can be observed that the performance of Pauli neighbors surpasses that of CPTP neighbors, suggesting that Pauli neighbors provide a better choice for PEC-inspired NIL. Moreover, we observe that the protocol based on ZNE neighbors also achieves competitive performance, even though it uses only four neighbor circuits per training circuit. It outperforms both CPTP and Pauli neighbors when the number of available neighbor circuits is limited. However, Pauli neighbors deliver the best performance when the number of neighbor circuits exceeds 250 (in this case, there are a total of 300 weight-1 neighbor circuits).

To combine the power of both ZNE neighbors and Pauli neighbors, we propose a new type of neighbor map called *ZNE + Pauli neighbors*. This *combine* map is constructed by combining these

two approaches as follows:

$$\text{combine} \left(\langle \tilde{C} \rangle_{\epsilon}, \langle \tilde{C} \rangle_{1.1\epsilon}, \langle \tilde{C} \rangle_{1.34\epsilon}, \langle \tilde{C} \rangle_{1.58\epsilon}, \langle \tilde{C}_1 \rangle, \dots, \langle \tilde{C}_N \rangle \right),$$

where ϵ is the original noise rate and C_1, \dots, C_N are the Pauli neighbors. Again, by employing Lasso regression with $\gamma = 5$, we test this new neighbor and observe that it performs well even with a very small number of neighbors. As shown in Fig. 11, this neighbor achieves a two-order-of-magnitude improvement in MSE compared to Pauli neighbors when the number of neighbors is small. This further demonstrates the flexibility of our approach.

H.2 Comparison Between Linear Models and Neural Networks

We first show that Lasso regression can significantly reduce the computational cost of learning-based QEM protocols compared to standard linear regression.

Table 2 illustrates the example of `vqe-6-4`. It can be seen that by adjusting the ℓ_1 norm constraint in Eq. (7), we can significantly reduce the sampling cost of the protocol, while the QEM performance only slightly decreases. It is critical to note that, as evidenced by the last column of Table 2, the value of $\sum_i |c_i|$ obtained by ordinary linear regression is extremely high, rendering it nearly unusable in practical applications. This issue stems from the ill-conditioning of the least squares coefficient matrix. However, implementing Lasso regression significantly reduces the value of $\sum_i |c_i|$, thereby greatly reducing the computational cost. Therefore, the advantage of Lasso regression deserves further investigation in learning-based QEM protocols.

γ	Training MSE	Test MSE	$\sum_i c_i $
unconstrained	8.17×10^{-7}	7.03×10^{-7}	11057.57
10	8.57×10^{-7}	7.93×10^{-7}	2.6
2	8.87×10^{-7}	8.97×10^{-7}	1.74
1.5	1.37×10^{-6}	1.54×10^{-6}	1.39

Table 2: Performance of the Lasso regression with different values of γ , where the target circuit is `vqe-6-4`.

In Fig. 12, we also compare the performance of our approach with neural network-based approaches. Here, the size of training circuits is set to 5,000. It turns out that in all cases we have studied, linear regression significantly outperforms neural networks in QEM performance, indicating that nonlinearity may not offer advantages in our tasks.

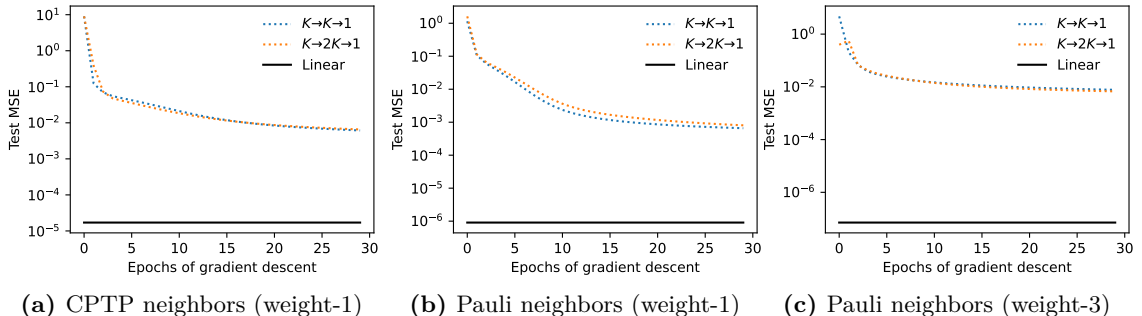


Figure 12: Comparisons between the performances of learning-based QME models with different neighbors and different learning models. Here neighbor circuits can be Pauli neighbors or CPTP neighbors, and learning models can be linear models or neural networks ($K \rightarrow K \rightarrow 1$ and $K \rightarrow 2K \rightarrow 1$). The target circuit is `vqe-6-4`.

I Quantum Chemistry Problems

Following the approach in Ref. [36], we study the LiH and F_2 molecular Hamiltonians. The Hamiltonians for both molecules are generated in the STO-3G basis set and then transformed into qubit Hamiltonians using the Jordan-Wigner transformation. This process is automatically implemented by the `qchem.molecular_hamiltonian` function in PennyLane [62] with the following specific settings. For LiH, we set

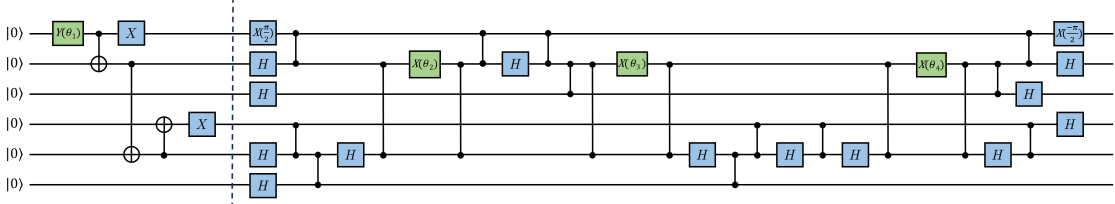
- `coordinates` = `[[0.3925, 0.0, 0.0], [-1.1774, 0.0, 0.0]]`,
- `active_electrons` = 2,
- `active_orbitals` = 3.

For F_2 , we set

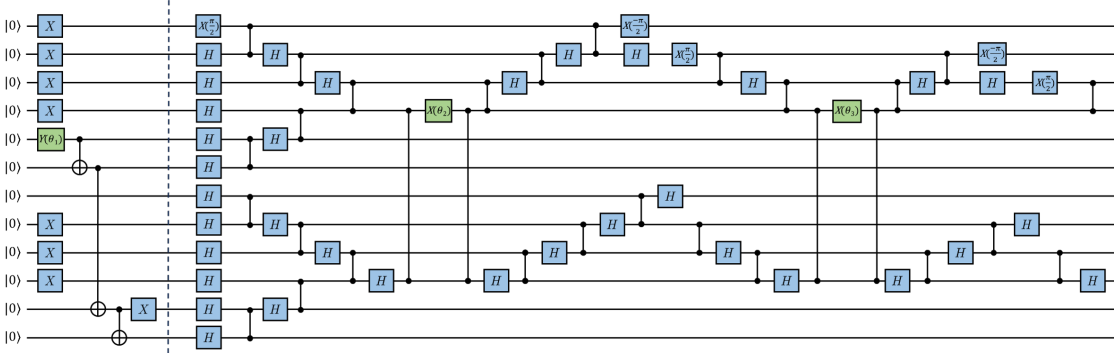
- `coordinates` = `[[0.0, 0.0, -0.7059], [0.0, 0.0, 0.7059]]`,
- `active_electrons` = 10,
- `active_orbitals` = 6.

The resulting Hamiltonian is 6-qubit for LiH and 12-qubit for F_2 .

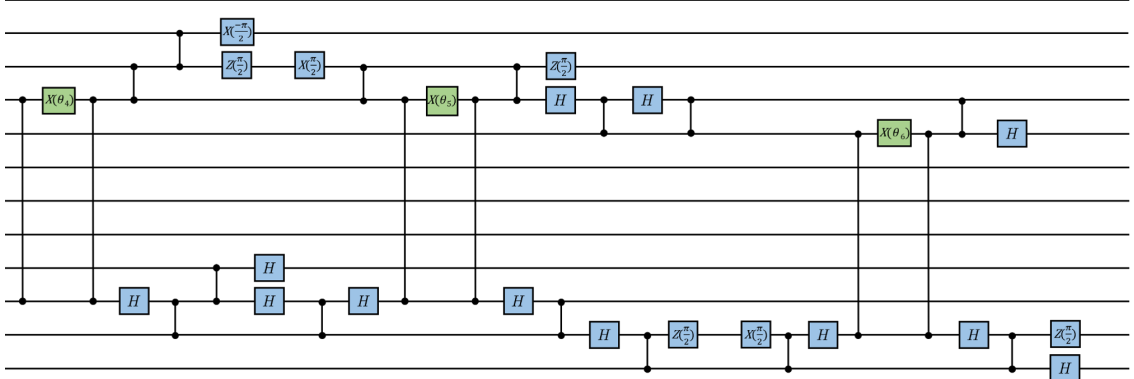
The ansatz circuits for VQE in both cases are chosen to be unitary-coupled clusters, where a series of circuit simplification and compilation strategies from Ref. [36] are applied. The ansatz circuit for LiH is shown in Fig. 13 (a) and that for F_2 is shown in Fig. 13 (b). The gates before the dotted lines form the quantum circuits for preparing the initial multi-reference states. Here, the parameterized gates are represented by the yellow blocks, which are all Pauli rotation gates.



(a) LiH



(b) F₂ part 1



(c) F₂ part 2

Figure 13: The compiled UCC ansatz circuits for LiH and F₂. The circuits in subfigure (b) and subfigure (c) together comprise the compiled UCC ansatz circuits for F₂. The part of the circuit before the blue dashed line represents the initial state preparation. The gates marked in green, along with all the two-qubit gates, are fixed Clifford gates, while the gates marked in yellow are single-parameter rotation gates.

I.1 Performance of NIL on UCC Ansatz Circuits for F₂

In this subsection, we demonstrate the application of our method to noise mitigation in UCC ansatz circuits for F₂, with the circuit diagrams shown in Fig. 13(b) and Fig. 13(c).

Specifically, we use only half of the weight-1 Pauli neighbors as the set of neighbor circuits, and then generate 1,000 training circuits by the 2-design training method. To obtain each noisy expectation value for the training circuits, we run each circuit 10,000 times and calculate the expectation value as the output. The label for each training circuit is the exact expectation value, which can be obtained efficiently since it is a Clifford circuit. Finally, we apply Lasso regression to fit the training set. As shown in Fig. 14, the training MSE (\approx test MSE) is nearly 10^{-4} , which is comparable to the statistical fluctuations caused by measurement shot noise. Compared with the

MSE of the noisy outputs (≈ 0.25), the mitigation gain reaches nearly two orders of magnitude, corresponding to a suppression of about 99% of the errors in terms of MSE. This numerical result demonstrates that our approach is applicable to real quantum chemistry tasks of modest size.

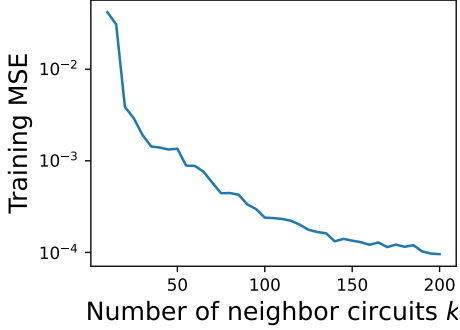


Figure 14: The 12-qubit UCC ansatz circuit for F_2 . In this case, the MSE of the noisy outputs without mitigation is 0.25.

References

- [1] Richard P. Feynman. Simulating physics with computers. *Int. J. Theor. Phys.*, 21(6-7):467–488, jun 1982.
- [2] S. Lloyd. Universal quantum simulators. *Science*, 273(5278):1073–1078, aug 1996.
- [3] P.W. Shor. Algorithms for quantum computation: discrete logarithms and factoring. In *Proceedings 35th Annual Symposium on Foundations of Computer Science*, pages 124–134, Santa Fe, NM, USA, 1994. IEEE Comput. Soc. Press.
- [4] Lov K. Grover. A fast quantum mechanical algorithm for database search. In *Proceedings of the twenty-eighth annual ACM symposium on Theory of computing - STOC '96*, pages 212–219, Philadelphia, Pennsylvania, United States, 1996. ACM Press.
- [5] John Preskill. Quantum Computing in the NISQ era and beyond. *Quantum*, 2:79, August 2018. arXiv: 1801.00862.
- [6] Kristan Temme, Sergey Bravyi, and Jay M. Gambetta. Error mitigation for short-depth quantum circuits. *Phys. Rev. Lett.*, 119(18):180509, November 2017. arXiv: 1612.02058.
- [7] Ying Li and Simon C. Benjamin. Efficient Variational Quantum Simulator Incorporating Active Error Minimization. *Phys. Rev. X*, 7(2):021050, June 2017.
- [8] Dorit Aharonov, Ori Albertron, Itai Arad, Yosi Atia, Eyal Bairey, Zvika Brakerski, Itsik Cohen, Omri Golan, Ilya Gurwich, Oded Kenneth, Eyal Leviatan, Netanel H. Lindner, Ron Aharon Melcer, Adiel Meyer, Gili Schul, and Maor Shutman. On the importance of error mitigation for quantum computation. arXiv:2503.17243, 2025.
- [9] X. Bonet-Monroig, R. Sagastizabal, M. Singh, and T. E. O’Brien. Low-cost error mitigation by symmetry verification. *Phys. Rev. A*, 98(6):062339, December 2018.
- [10] Sam McArdle, Xiao Yuan, and Simon Benjamin. Error-Mitigated Digital Quantum Simulation. *Phys. Rev. Lett.*, 122(18):180501, May 2019.
- [11] William J. Huggins, Sam McArdle, Thomas E. O’Brien, Joonho Lee, Nicholas C. Rubin, Sergio Boixo, K. Birgitta Whaley, Ryan Babbush, and Jarrod R. McClean. Virtual Distillation for Quantum Error Mitigation. *Phys. Rev. X*, 11(4):041036, November 2021.

[12] Bálint Koczor. Exponential Error Suppression for Near-Term Quantum Devices. *Phys. Rev. X*, 11(3):031057, September 2021.

[13] Zhenhuan Liu, Xingjian Zhang, Yue-Yang Fei, and Zhenyu Cai. Virtual channel purification. *arXiv preprint arXiv:2402.07866*, 2024.

[14] Haoran Liao, Derek S Wang, Iskandar Situdikov, Ciro Salcedo, Alireza Seif, and Zlatko K Minev. Machine learning for practical quantum error mitigation. *Nature Machine Intelligence*, pages 1–9, 2024.

[15] Piotr Czarnik, Andrew Arrasmith, Patrick J. Coles, and Lukasz Cincio. Error mitigation with Clifford quantum-circuit data. *Quantum*, 5:592, November 2021. arXiv:2005.10189.

[16] Armands Strikis, Dayue Qin, Yanzhu Chen, Simon C. Benjamin, and Ying Li. Learning-Based Quantum Error Mitigation. *PRX Quantum*, 2(4):040330, November 2021. arXiv: 2005.07601.

[17] Angus Lowe, Max Hunter Gordon, Piotr Czarnik, Andrew Arrasmith, Patrick J. Coles, and Lukasz Cincio. Unified approach to data-driven quantum error mitigation. *Phys. Rev. Research*, 3(3):033098, July 2021.

[18] Abhinav Kandala, Kristan Temme, Antonio D. Córcoles, Antonio Mezzacapo, Jerry M. Chow, and Jay M. Gambetta. Error mitigation extends the computational reach of a noisy quantum processor. *Nature*, 567(7749):491–495, March 2019.

[19] Youngseok Kim, Christopher J. Wood, Theodore J. Yoder, Seth T. Merkel, Jay M. Gambetta, Kristan Temme, and Abhinav Kandala. Scalable error mitigation for noisy quantum circuits produces competitive expectation values. *Nat. Phys.*, February 2023. arXiv:2108.09197.

[20] Ryuji Takagi. Optimal resource cost for error mitigation. *Phys. Rev. Research*, 3(3):033178, August 2021.

[21] Ryuji Takagi, Suguru Endo, Shintaro Minagawa, and Mile Gu. Fundamental limits of quantum error mitigation, March 2021. arXiv:2109.04457 [quant-ph].

[22] Jiaqing Jiang, Kun Wang, and Xin Wang. Physical implementability of linear maps and its application in error mitigation. *Quantum*, 5:600, 2021.

[23] Ewout Van Den Berg, Zlatko K Minev, Abhinav Kandala, and Kristan Temme. Probabilistic error cancellation with sparse pauli–lindblad models on noisy quantum processors. *Nature physics*, 19(8):1116–1121, 2023.

[24] Alberto Peruzzo, Jarrod McClean, Peter Shadbolt, Man-Hong Yung, Xiao-Qi Zhou, Peter J. Love, Alán Aspuru-Guzik, and Jeremy L. O’Brien. A variational eigenvalue solver on a photonic quantum processor. *Nat. Commun.*, 5(1):4213, September 2014.

[25] M.-H. Yung, J. Casanova, A. Mezzacapo, J. McClean, L. Lamata, A. Aspuru-Guzik, and E. Solano. From transistor to trapped-ion computers for quantum chemistry. *Sci Rep*, 4(1):3589, January 2014.

[26] Jarrod R. McClean, Jonathan Romero, Ryan Babbush, and Alán Aspuru-Guzik. The theory of variational hybrid quantum-classical algorithms. *New Journal of Physics*, 18(2):023023, 2016.

[27] Abhinav Kandala, Antonio Mezzacapo, Kristan Temme, Maika Takita, Markus Brink, Jerry M. Chow, and Jay M. Gambetta. Hardware-efficient variational quantum eigensolver for small molecules and quantum magnets. *Nature*, 549:242–246, 2017.

[28] Edward Farhi, Jeffrey Goldstone, and Sam Gutmann. A Quantum Approximate Optimization Algorithm. *arXiv:1411.4028*, November 2014. arXiv: 1411.4028.

[29] Edward Farhi and Aram W Harrow. Quantum supremacy through the quantum approximate optimization algorithm. *arXiv preprint arXiv:1602.07674*, 2016.

[30] Nikolaj Moll, Panagiotis Barkoutsos, Lev S Bishop, Jerry M Chow, Andrew Cross, Daniel J Egger, Stefan Filipp, Andreas Fuhrer, Jay M Gambetta, Marc Ganzhorn, et al. Quantum optimization using variational algorithms on near-term quantum devices. *Quantum Science and Technology*, 3(3):030503, 2018.

[31] Suguru Endo, Simon C. Benjamin, and Ying Li. Practical Quantum Error Mitigation for Near-Future Applications. *Phys. Rev. X*, 8(3):031027, July 2018. arXiv:1712.09271.

[32] Daniel Gottesman. The Heisenberg Representation of Quantum Computers. In *Group22: Proceedings of the XXII International Colloquium on Group Theoretical Methods in Physics*, pages 32–43, Cambridge, MA, 1999. arXiv: quant-ph/9807006.

[33] Scott Aaronson and Daniel Gottesman. Improved Simulation of Stabilizer Circuits. *Phys. Rev. A*, 70(5):052328, November 2004. arXiv: quant-ph/0406196.

[34] Youngseok Kim, Andrew Eddins, Sajant Anand, Ken Xuan Wei, Ewout Van Den Berg, Sami Rosenblatt, Hasan Nayfeh, Yantao Wu, Michael Zaletel, Kristan Temme, et al. Evidence for the utility of quantum computing before fault tolerance. *Nature*, 618(7965):500–505, 2023.

[35] Dave Wecker, Matthew B. Hastings, and Matthias Troyer. Progress towards practical quantum variational algorithms. *Phys. Rev. A*, 92(4):042303, October 2015.

[36] Shaojun Guo, Jinzhao Sun, Haoran Qian, Ming Gong, Yukun Zhang, Fusheng Chen, Yangsen Ye, Yulin Wu, Sirui Cao, Kun Liu, Chen Zha, Chong Ying, Qingling Zhu, He-Liang Huang, Youwei Zhao, Shaowei Li, Shiyu Wang, Jiale Yu, Daojin Fan, Dachao Wu, Hong Su, Hui Deng, Hao Rong, Yuan Li, Kaili Zhang, Tung-Hsun Chung, Futian Liang, Jin Lin, Yu Xu, Lihua Sun, Cheng Guo, Na Li, Yong-Heng Huo, Cheng-Zhi Peng, Chao-Yang Lu, Xiao Yuan, Xiaobo Zhu, and Jian-Wei Pan. Experimental quantum computational chemistry with optimised unitary coupled cluster ansatz. *Nat. Phys.*, 20(8):1240–1246, August 2024.

[37] Wataru Inoue, Koki Aoyama, Yusuke Teranishi, Keita Kanno, Yuya O. Nakagawa, and Kosuke Mitarai. Almost optimal measurement scheduling of molecular hamiltonian via finite projective plane. *Phys. Rev. Res.*, 6:013096, Jan 2024.

[38] John A Pople. Nobel lecture: Quantum chemical models. *Reviews of Modern Physics*, 71(5):1267, 1999.

[39] James Kirkpatrick, Brendan McMorrow, David HP Turban, Alexander L Gaunt, James S Spencer, Alexander GDG Matthews, Annette Obika, Louis Thiry, Meire Fortunato, David Pfau, et al. Pushing the frontiers of density functionals by solving the fractional electron problem. *Science*, 374(6573):1385–1389, 2021.

[40] Robert Tibshirani. Regression shrinkage and selection via the lasso. *Journal of the Royal Statistical Society Series B: Statistical Methodology*, 58(1):267–288, 1996.

[41] MOSEK ApS, 2024. <https://docs.mosek.com/latest/faq/index.html>.

[42] Ryan LaRose, Andrea Mari, Sarah Kaiser, Peter J. Karalekas, Andre A. Alves, Piotr Czarnik, Mohamed El Mandouh, Max H. Gordon, Yousef Hindy, Aaron Robertson, Purva Thakre, Misty Wahl, Danny Samuel, Rahul Mistri, Maxime Tremblay, Nick Gardner, Nathaniel T. Stemen, Nathan Shammah, and William J. Zeng. Mitiq: A software package for error mitigation on noisy quantum computers. *Quantum*, 6:774, Aug 2022.

[43] Ruiqi Zhang, Xiaodie Lin, Zhenyu Chen, and Zhaohui Wei. Zero-noise extrapolation enhanced by clifford circuits. Manuscript in preparation, 2025.

[44] Craig Gidney. Stim: a fast stabilizer circuit simulator. *Quantum*, 5:497, July 2021.

[45] D. Gross, K. Audenaert, and J. Eisert. Evenly distributed unitaries: on the structure of unitary designs. *Journal of Mathematical Physics*, 48(5):052104, May 2007. arXiv:quant-ph/0611002.

[46] Piotr Czarnik, Andrew Arrasmith, Patrick J Coles, and Lukasz Cincio. Error mitigation with clifford quantum-circuit data. *Quantum*, 5:592, 2021.

[47] F. Pedregosa, G. Varoquaux, A. Gramfort, V. Michel, B. Thirion, O. Grisel, M. Blondel, P. Prettenhofer, R. Weiss, V. Dubourg, J. Vanderplas, A. Passos, D. Cournapeau, M. Brucher, M. Perrot, and E. Duchesnay. Scikit-learn: Machine learning in python. *Journal of Machine Learning Research*, 12:2825–2830, 2011.

[48] Åke Björck. *Numerical Methods for Least Squares Problems*. SIAM, Philadelphia, 1996.

[49] Stephen Boyd and Lieven Vandenberghe. *Convex optimization*. Cambridge university press, 2004.

[50] Roger Penrose. A generalized inverse for matrices. In *Mathematical proceedings of the Cambridge philosophical society*, volume 51, pages 406–413. Cambridge University Press, 1955.

[51] Andrew Y Ng. Feature selection, l_1 vs. l_2 regularization, and rotational invariance. In *Proceedings of the twenty-first international conference on Machine learning*, page 78, 2004.

[52] Arthur E. Hoerl and Robert W. Kennard. Ridge regression: Biased estimation for nonorthogonal problems. *Technometrics*, 12(1):55–67, 1970.

[53] Gene H Golub, Per Christian Hansen, and Dianne P O’Leary. Tikhonov regularization and total least squares. *SIAM journal on matrix analysis and applications*, 21(1):185–194, 1999.

[54] Mehryar Mohri. Foundations of machine learning, 2018.

[55] Mark Schmidt. Least squares optimization with l_1 -norm regularization. *CS542B Project Report*, 504(2005):195–221, 2005.

[56] Julien Mairal and Bin Yu. Complexity analysis of the lasso regularization path. *arXiv preprint arXiv:1205.0079*, 2012.

[57] Volker Roth. The generalized lasso. *IEEE transactions on neural networks*, 15(1):16–28, 2004.

[58] Elad Hazan and Tomer Koren. Linear regression with limited observation. *arXiv preprint arXiv:1206.4678*, 2012.

[59] Dayue Qin, Yanzhu Chen, and Ying Li. Error statistics and scalability of quantum error mitigation formulas. *npj Quantum Information*, 9(1):35, 2023.

[60] Igor L. Markov and Yaoyun Shi. Simulating Quantum Computation by Contracting Tensor Networks. *SIAM J. Comput.*, 38(3):963–981, January 2008. arXiv: quant-ph/0511069.

[61] Zak Webb. The clifford group forms a unitary 3-design. *arXiv preprint arXiv:1510.02769*, 2015.

[62] Ville Bergholm, Josh Izaac, Maria Schuld, Christian Gogolin, Shahnawaz Ahmed, Vishnu Ajith, M. Sohaib Alam, Guillermo Alonso-Linaje, B. AkashNarayanan, Ali Asadi, Juan Miguel Arrazola, Utkarsh Azad, Sam Banning, Carsten Blank, Thomas R Bromley, Benjamin A. Cordier, Jack Cerone, Alain Delgado, Olivia Di Matteo, Amintor Dusko, Tanya Garg, Diego Guala, Anthony Hayes, Ryan Hill, Aroosa Ijaz, Theodor Isacsson, David Ittah, Soran Jahangiri, Prateek Jain, Edward Jiang, Ankit Khandelwal, Korbinian Kottmann, Robert A. Lang, Christina Lee, Thomas Loke, Angus Lowe, Keri McKiernan, Johannes Jakob Meyer, J. A. Montañez-Barrera, Romain Moyal, Zeyue Niu, Lee James O’Riordan, Steven Oud, Ashish Panigrahi, Chae-Yeon Park, Daniel Polatajko, Nicolás Quesada, Chase Roberts, Nahum Sá, Isidor Schoch, Borun Shi, Shuli Shu, Sukin Sim, Arshpreet Singh, Ingrid Strandberg, Jay Soni, Antal Száva, Slimane Thabet, Rodrigo A. Vargas-Hernández, Trevor Vincent, Nicola Vitucci, Maurice Weber, David Wierichs, Roeland Wiersema, Moritz Willmann, Vincent Wong, Shaoming Zhang, and Nathan Killoran. PennyLane: Automatic differentiation of hybrid quantum-classical computations, 2022.